HHS Public Access

Author manuscript

Cell Rep. Author manuscript; available in PMC 2021 March 11.

Published in final edited form as:

Cell Rep. 2021 January 26; 34(4): 108681. doi:10.1016/j.celrep.2020.108681.

Sexual and asexual development: two distinct programs producing the same tunicate

Mark Kowarsky[1,10], **Chiara Anselmi**[2,3,4,10], **Kohji Hotta**[5], **Paolo Burighel**[2], **Giovanna Zaniolo**[2], **Federico Caicci**[2], **Benyamin Rosental**[3,4,6], **Norma F. Neff**[7], **Katherine J. Ishizuka**[3,4], **Karla J. Palmeri**[3,4], **Jennifer Okamoto**[7], **Tal Gordon**[8], **Irving L. Weissman**[3,4,7,11], **Stephen R. Quake**[7,9,11], **Lucia Manni**[2,11,*], **Ayelet Voskoboynik**[3,4,7,11,12,*]

[1]Department of Physics, Stanford University, Stanford, CA 94305, USA

[2]Dipartimento di Biologia, Università degli Studi di Padova, 35122 Padova, Italy

[3]Institute for Stem Cell Biology and Regenerative Medicine, and Ludwig Center, Stanford University School of Medicine, Stanford, CA 94305, USA

[4]Department of Biology, Stanford University, Hopkins Marine Station, Pacific Grove, CA 93950, USA

[5]Department of Biosciences and Informatics, Keio University, Yokohama 223-8522, Japan

[6]The Shraga Segal Department of Microbiology, Immunology and Genetics, Faculty of Health Sciences, Center for Regenerative Medicine and Stem Cells, Ben-Gurion University of the Negev, Beer-Sheva 84105, Israel

[7]Chan Zuckerberg Biohub, San Francisco, CA 94158, USA

[8]Zoology Department, Tel Aviv University, Tel Aviv 69978, Israel

[9]Departments of Applied Physics and Bioengineering, Stanford University, Stanford, CA 94305, USA

[10]These authors contributed equally

[11]These authors contributed equally

[12]Lead contact

SUMMARY

*Correspondence: lucia.manni@unipd.it (L.M.), ayeletv@stanford.edu (A.V.).

AUTHOR CONTRIBUTIONS

Conception and design, A.V., M.K., L.M., and C.A.; mariculture and sample collection, K.J.I. and K.J.P.; RNA library preparation, K.J.P. and A.V.; sequencing, J.O. and N.F.N.; sequencing analysis and development of analytical tools, M.K. and S.R.Q.; light, electron, confocal, and two-photon microscopy, L.M., P.B., G.Z., F.C., C.A., K.H., T.G., and A.V.; 3D reconstruction, L.M. and F.C.; FACS, B.R.; writing of the manuscript, M.K., A.V., L.M., C.A., K.J.P., K.J.I., and I.L.W.; technical support and conceptual advice, K.H., N.F.N., S.R.Q., and I.L.W.

SUPPLEMENTAL INFORMATION

Supplemental Information can be found online at https://doi.org/10.1016/j.celrep.2020.108681.

DECLARATIONS OF INTERESTS

The authors declare no competing interests.

Colonial tunicates are the only chordate that possess two distinct developmental pathways to produce an adult body: either sexually through embryogenesis or asexually through a stem cell-mediated renewal termed blastogenesis. Using the colonial tunicate *Botryllus schlosseri*, we combine transcriptomics and microscopy to build an atlas of the molecular and morphological signatures at each developmental stage for both pathways. The general molecular profiles of these processes are largely distinct. However, the relative timing of organogenesis and ordering of tissue-specific gene expression are conserved. By comparing the developmental pathways of *B. schlosseri* with other chordates, we identify hundreds of putative transcription factors with conserved temporal expression. Our findings demonstrate that convergent morphology need not imply convergent molecular mechanisms but that it showcases the importance that tissue-specific stem cells and transcription factors play in producing the same mature body through different pathways.

Graphical Abstract

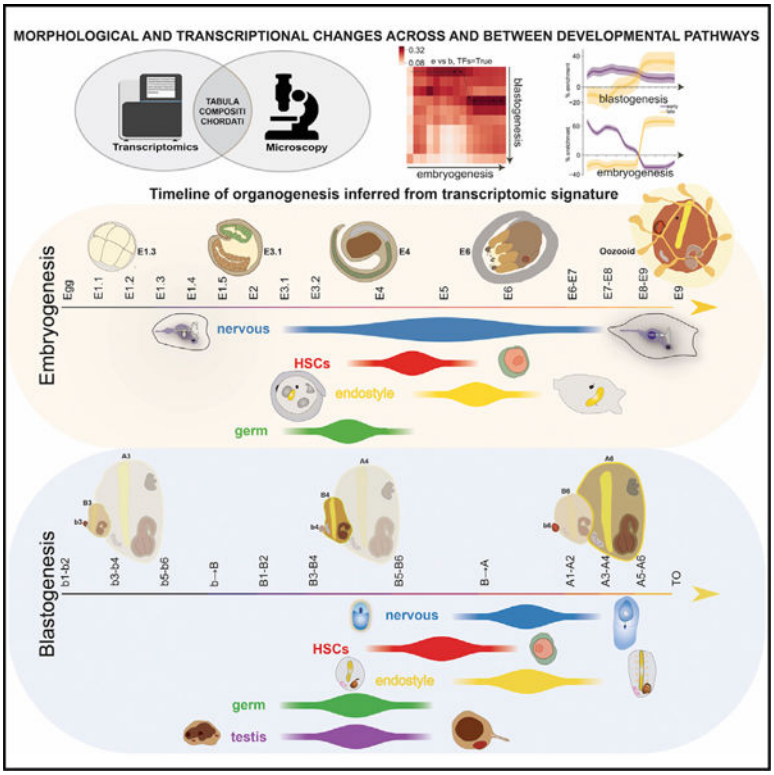

In Brief

Kowarsky et al. present a developmental atlas of colonial tunicates. They show how sexual and asexual reproduction processes, despite having largely distinct molecular programs, share similar timing of organ formation. Tissue-specific stem cells and transcription factors display similar genetic dynamics in different developmental pathways to produce the same organism.

INTRODUCTION

Most multicellular organisms develop sexually via a single fertilized egg (embryogenesis), or via an asexual reproduction process in which offspring develop as an outgrowth of their parent body (blastogenesis). While some organisms can reproduce both ways, others are restricted to one. Decades of studies on embryogenesis across deuterostomes traced the fate of specific cell lineages and revealed transcriptional blueprints of embryogenesis (Bosch, 2009; Cao et al., 2019; Chan et al., 2018; Conklin, 1905; Farrell et al., 2018; Nowotschin et al., 2019; Schaum et al., 2018; Sulston et al., 1983; Wagner et al., 2018). Blastogenesis studies describe the life cycle and isolation of putative stem cells that mediate organogenesis, but they do not include a comprehensive study of the molecular programs that regulate blastogenesis (Gasparini et al., 2011; Laird et al., 2005; Manni et al., 2019; Rinkevich et al., 2013; Rosental et al., 2018; Tiozzo et al., 2005; Voskoboynik et al., 2008). The relationship between embryogenesis and blastogenesis, and what, if any, unifying principles govern these distinct developmental pathways, remains a mystery.

Colonial tunicates are a key to solving this mystery. These marine organisms are unique among chordates: they can produce their adult body through two pathways (Figures 1A, 1B, 2A, and S1), and they possess whole body regenerative capabilities (Alié et al., 2020; Gasparini et al., 2014; Manni et al., 2019; Voskoboynik et al., 2007). A colony of the tunicate *Botryllus schlosseri* contains many individuals (zooids), derived by asexual reproduction from a single metamorphosed larva. These clonal progenies lie inside a gelatinous tunic connected by extracorporeal blood vessels (Figure 1C). Sexual development begins with fertilization of an egg by free-swimming sperm, creating a zygote. It develops during the next 6 days (at 18°C) inside the zooid, until released as a swimming larva (Video S1). The larva features chordate characteristics such as a notochord, dorsal neural tube, ventral endoderm, segmented musculature in the tail, photolith, and larval brain. The hatched larva swims to subtidal surfaces, settles, and metamorphoses into an invertebrate-like organism, the oozooid. The latter has already produced buds, the precursors for the next generation's zooid (blastozooid), initiating a weekly asexual budding cycle: secondary buds grow into primary buds that in turn complete organogenesis and replace their parent zooid (Video S2). At the end of the cycle, the parent zooids in the colony undergo synchronized cell removal and are resorbed through phagocytosis, a process that eliminates most cells, excluding the stem cells (Laird et al., 2005; Rinkevich et al., 2013; Rosental et al., 2018; Voskoboynik et al., 2008).

During embryogenesis, a single fertilized egg differentiates and divides into various lineages that form the adult body. Blastogenesis differs in origin but similarly establishes body axis and organ formation (Figure 2A). The expression pattern of very few genes was comparatively studied in both embryogenesis and blastogenesis (Gasparini et al., 2011, 2014; Tiozzo et al., 2005). Therefore, we investigated comprehensively whether the convergent morphology of oozooids and blastozooids implies convergent molecular mechanisms, how organogenesis compares between sexual and asexual processes, and how the stem cells mediating these processes vary. We generated comprehensive whole transcriptomes and developed a bioinformatics method to identify developmentally dynamic genes (Methods S1; Figure 1D). Coupling this with confocal, two photon, light, and electron

microscopy, we characterized the stages of embryonic and blastogenetic development. For every stage, we identified unique and shared molecular characteristics, measured gene expression patterns of specific tissues or enriched stem cells populations, and identified the developmental origin of hematopoiesis, germ cells, and the central nervous system (CNS). This study generated *Tabula compositi chordati Botrylli*, a morphogenetic atlas of sexual and asexual development (Tables S1, S2, S3, S4, S5, S6, and S7).

This atlas demonstrates that the general transcriptomic landscapes of these processes are largely distinct, apart from two specific shared elements. First, the tissue-specific progenitor cells in blastogenesis and embryogenesis express similar gene sets. Second, in both embryogenesis and blastogenesis, tissues are formed in a similar order. When comparing the *Botryllus* pathways to embryogenesis in other chordates we identified putative transcription factors (TFs) that preserved their temporal expression throughout development stages. This study proves that distinct molecular programs can lead to the same outcome and also suggests that adult stem cells originate from specific embryonic precursor cells, showcasing the importance that stem cells must play in producing the same mature body through different pathways.

RESULTS

Tabula compositi chordati Botrylli, a morphogenetic atlas of sexual and asexual development

To study the molecular and morphological signatures associated with embryogenesis and blastogenesis, we compared developing embryos and buds at key developmental stages. In embryogenesis, specimens were taken from 15 different developmental stages across 7 days (Figure 1A). In blastogenesis, secondary buds, primary buds, combinations of primary and secondary buds, and adult zooids were taken from 12 developmental stages during a period of 7 days (Figure 1B). Corresponding samples taken for multiple imaging methods built the morphological atlas (Figure 1E). To identify tissue/cell-specific signatures, we sequenced different tissues, organs, and cell populations taken from zooids, including: dissected testes, endostyles, and brains (CNS); flow cytometry sorted enriched hematopoietic stem cells (HSCs) and candidate germline stem cells (cGSCs); and blood vessels embedded within the tunic (Figures 1F and S2; n = 27). A detailed morphological description of all stages was compiled based on the multiple imaging methods (Table S1). To simplify the comparison between *B. schlosseri*'s two developmental pathways and embryogenesis in other chordate species, stage names that refer to the day of development for embryo, secondary bud, primary bud, and adult zooid were used (Figures 1A, 1B, and 2A; Table S1). Reconstructions were made in 3D of a larva in early metamorphosis, an oozooid, and a primary bud and secondary bud, and their organs and tissues can be visualized in the MorphoNet browser (Figures 1G–1I and S1) (Leggio et al., 2019). To identify differentially expressed genes between all possible combinations of contiguous and individual developmental stages, we used edgeR (Robinson et al., 2010) and a new method we developed (see STAR methods; Methods S1; Figure 1D). Based on these analyses, a binary gene-time expression matrix for every expressed gene recorded along the developmental pathways was produced (Table S3).

Embryogenesis and blastogenesis have distinct molecular and morphological programs

Embryogenesis and blastogenesis have vastly different morpho-logical patterns that nonetheless produce similar adult bodies (Figures 1A, 1B, and 2A; Table S1). To reveal periods of similar and distinct gene expression patterns in a comprehensive and unbiased manner, we generated enrichment plots (STAR methods; Methods S2; Figures 2B–2E). These show the relative enrichment of a set of genes (compared to a baseline of a random set of the same number of genes) among the activated genes at a particular time. Within embryogenesis, the highest degree of similarity was between adjacent times as expected by the overall gradual and unidirectional nature of this process (Figure 2B). Similarly, in blastogenesis, the greatest transcriptional correlations occurred between adjacent times (Figure 2E), but in contrast to embryogenesis it has discontinuities. This is due to both the longer time periods between samples and the combining of secondary buds (b1–b4) and their parental tissue (primary bud [B]1–B4) in early stages of blastogenesis (Figure 1B). The genes specific to these time periods that have human or mouse gene homologs (Voskoboynik et al., 2013a) were analyzed using GeneAnalytics (Ben-Ari Fuchs et al., 2016), a tool that integrates multiple databases to match gene lists with the relevant Gene Ontology (GO) and pathways. These multi-gene enrichment analyses revealed the timing and expression patterns of hundreds of pathways, constituting the molecular blueprint of embryogenesis and blastogenesis (Tables S2, S3, S4, S5, and S6).

The first embryonic period, characterized by the first three cleavages, is typical in all tunicates (Conklin, 1905; Hotta et al., 2007; Satou and Satoh, 1999; Stach and Anselmi, 2015), and it expresses a unique molecular profile that significantly differs from later stages (Figure 2B). We hypothesize that this is in part due to the maternal-to-zygotic transition (Lee et al., 2013), the period during which a developing embryo begins to generate its own transcripts rather than using those inherited maternally. This unique profile also reflects the relatively short time where all cells are totipotent. Among the top pathways uniquely enriched at these early stages are key signaling pathways associated with cell proliferation, differentiation, and DNA activation and repair. Several pathways associated with the immune response are also uniquely enriched at this period, including interferon (IFN)-gamma signaling, antigen processing cross-presentation, and interleukin (IL)-2 pathways, suggesting a key role for immune signaling to embryonic cell differentiation (two to eight cells; Table S4).

Following early development, the morula (embryonic day [E] 1.4) and blastula (E1.5) stages lead into the formation of three germ layers in gastrula (E2) and to the development of the chordate neural plate during the neurula (E3.1) stage (Table S1A). Pathways associated with the nervous system, including the brain-derived neurotrophic factor signaling pathway, are first expressed during gastrula and neurula stages, correlating with the timing of the development of the neural plate (Table S4).

The tailbud (pear) stage (E3.2) leads to the formation of the tail, and in the wrap stages (E4–E6), the tail and trunk regions are separated and the heart, digestive system, branchial and peribranchial chambers, larval brain, notochord, nerve cord, rudiment of the adult brain, striated muscles, and ampullae are formed (Tables S1A and S1C). Correlating with the diverse tissues and organs developed during these stages, pathways associated with

cytoskeleton remodeling, mesodermal commitment, striated muscle contraction, and more are activated (Table S4).

The larva completes its development during the wrap stage and hatches before the zooids in their parental colony get resorbed (E7; Figure 2A). A larval brain containing a photolith connected to three sensory papillae, and a tail with notochord and segmented musculature allow the larva to swim and settle on a subtidal surface, after which the larva brain and tail are resorbed (Caicci et al., 2010). All other larval organs and tissues, including brain, oral siphons, and atrial siphons; a branchial sac with stigmata and endostyle; a digestive system with an esophagus, stomach, and intestine; eight ampullae; and two buds, persist after metamorphosis (Figures 1G and 1H; Table S1A). The mTOR pathway, a central regulator of mammalian metabolism and physiology, and the Rho guanosine diphosphate-dissociation inhibitor (RhoGDI) pathway, which is associated with diverse aspects of cellular regulation, including gene transcription, cell cycle progression, phagocytosis, and vesicular traffic, are uniquely activated during the larva stage (E6–E7). During the transition from larva to oozooid, when the tail and the larva brain are lost, pathways associated with calcium reabsorption and oxidative stress are activated (E8–E9; Tables S1A and S4). This period is also characterized by activation of pathways associated with cardiac conduction, fructose and mannose metabolism, the apelin signaling pathway, and development of ligand-independent activation of the ESR1 and ESR2 pathways, reflecting morphological and physiological changes observed in this stage, including the formation of tunic and new blood vessels and robust heart activity (Table S4).

Within blastogenesis, the peribranchial epidermis closes to form an inner vesicle, surrounded by the parental epidermis (outer vesicle) in order to create the secondary bud epidermis (Figures 1I and 2A; Table S1B) (Manni et al., 2014), while circulating hemocytes originated from the colony stem cell niches migrate to the developing secondary buds (Rinkevich et al., 2013; Rosental et al., 2018; Voskoboynik et al., 2008). During the first week of development (b1 to b→B) all organ rudiments are formed in the buds, including branchial and peribranchial chambers, intestine, heart, and the nervous system. A few pathways that are expressed in early stages of embryogenesis are also activated in early stages of blastogenesis, including P53, ATM, HSF1-dependent transactivation, IFN-gamma signaling, antigen processing cross-presentation, and IL-2, suggesting a key role of these pathways in early development of both programs (Table S5B).

In primary buds the organs complete their differentiation and enlarge to prepare the primary bud for transformation into a functional filter feeding adult zooid (B→A). The FOXO family signaling pathway that is associated with cell cycle control, apoptosis, oxidative stress resistance and longevity, and the TRK receptor signaling pathway, associated with neuronal survival and differentiation, are among the uniquely expressed pathways in this transition stage (Tables S1B and S5). The zooid undergoes relatively minor growth and morphological changes, while pathways associated with metabolism, homeostasis, immunity, and circadian entrainment are highly expressed (A1–A6; Table S5). Pathways associated with stem cell pluripotency and development, including Wnt, Hedgehog, Notch, fibroblast growth factor receptor (FGFR), and epidermal growth factor receptor (EGFR), are also highly expressed during A1–A6, pointing to maintenance and activity of stem cells

before they migrate to budding niches (Table S5). Zooid replacement occurs at the end of this era (takeover [TO]), with all zooids in a colony degenerating in a synchronized wave of massive apoptosis and phagocytic cell removal (Table S1B) (Ballarin et al., 2008; Lauzon et al., 1993). While stages A1–A6 share a highly similar transcriptional profile, the TO profile differs significantly from those stages (Figure 2E). About 30 pathways unique to TO were detected, and they include those associated with complement and coagulation cascades, GAP junction trafficking, glycan degradation, and vitamin digestion and absorption, all correlating with the events observed during TO (Table S5).

Embryogenesis and blastogenesis are highly dissimilar to each other despite the shared body plan, organs, and tissues that develop. To directly compare them, we calculated the enrichment of activated genes using the same method described above for a single developmental pathway (STAR methods; Methods S2; Figures 2C and 2D). These two pathways express similar gene numbers, but they are highly dissimilar, with a maximum enrichment of only about 30%. Interestingly, genes that are co-expressed are more likely to have vertebrate homologs, indicating that shared developmental genes are more likely to be conserved between developmental programs than those in a specific program.

The first embryonic stages (E1.1–E1.3) are distinct from all blastogenic stages (Figure 2D), suggesting that this period of initial cleavage does not have any correspondence in blastogenesis. Likewise, the periods during TO (B→A and TO) have transcriptional profiles distinct from those of any embryonic stage (Figure 2C; Table S5). This is in part expected, since they are events marking a discontinuity in an individual's life that does not have any correspondence in embryogenesis. The TO has no correspondence with metamorphosis, during which larval tissue resorption is also governed by apoptosis (Karaiskou et al., 2015). High numbers of genes from the apoptosis and survival caspase cascade pathway are expressed both in the resorbing zooids (TO) and during metamorphosis (E8); however, this pathway is also activated during other embryonic and blastogenesis stages (E2–E8; b→B; B→A; TO). Although embryogenesis and blastogenesis can be considered transcriptionally distinct, they share several biological pathways (Table S5B). However, the particular genes from a specific pathway that are expressed at each of the developmental programs and their expression timing vary significantly (Tables S4A–S4L and S5A–S5P).

There are two blocks of stages with shared expression: (1) embryonic stages of morula (E1.4) to early wrap (E4) with the blastogenic stages of secondary bud to primary bud and secondary bud (b1–B4), and (2) embryonic stages from mid wrap (E5) to oozooid (E9) with the adult zooids (A1–A6). From a morphological point of view (Table S1), the first block shows the organization of the body plan, whereas the second block has adult organs in comparable mature states. We hypothesized that the shared expression during early development is partially derived from stem cells. Indeed, when we looked at the expression of known mammalian embryonic stem cells, pluripotency genes, and lineage differentiation genes, we found many that were co-expressed in the early time periods, including homologs to genes from the *Wnt*, *Smad*, *Pou*, *Sox*, *Tbx*, *Cdx*, *Hnf*, *Otx*, *Zic*, *Bmp*, *Fgf*, *Mapk*, *Kdr*, *Sirt*, and *Fox* families (Table S3F). The shared expression during the second block is derived from enrichment of pathways associated with metabolism, homeostasis, and growth (Table S5B).

Organ-enriched molecular profiles correlate with morphogenesis

To identify and compare the developmental origin of specific organs and tissues during embryogenesis and blastogenesis we used detailed morphological data and tissue- and cell type-specific transcriptomes of the nervous system, hematopoietic system, and endostyle and reproductive system (testis) (Figure S2; Tables S1C and S3E). For each organ and cell type, the relative enrichment of genes associated with that tissue was computed along the developmental pathways (see STAR Methods; Methods S2; Figures 3, 4, 5, and 6). We compared varying regions to concurrent morphological changes to find genes that may drive these changes, including putative TFs that may precede or drive organ development.

Origin of the nervous system

B. schlosseri forms two brains during its chordate embryonic development: (1) a specific larval brain, and (2) a second brain (cerebral ganglion) connected to the first that persists in the oozooid after metamorphosis when the larval brain degenerates. During the embryonic phase, a bud also developed and remains after metamorphosis in the oozooid. In this bud the nervous system of the next-generation zooid is formed. The larval brain responds to light and gravity, controls muscle contractions in the tail, and directs larval settlement. When larvae settle, they often place themselves near histocompatible partners (partners sharing at least one BHF allele; Grave and Woodbridge, 1924; Grosberg and Quinn, 1986; Voskoboynik et al., 2013b), improving the chances of successfully forming a chimera, likely utilizing olfactory-like sensory input to guide them. The zooid brain functions during the sessile invertebrate stage, controlling siphons, branchial sac stigmata, and body muscle contractions. It may also control *B. schlosseri*'s weekly blastogenic cycles as well as neurogenesis. Long-term memories would be surprising as the brain is regenerated from stem/progenitor cells each cycle.

The larval nervous system anatomy differs in a significant way from the invertebrate sessile zooid nervous system. The larval brain includes a small ganglionic vesicle connected to a visceral ganglion, a neck, and a nerve cord. It is also connected to a large sensory vesicle with a photolith containing six photoreceptor cells, a statocyst, and other specialized cells that detect light and gravity (Manni et al., 1999; Sorrentino et al., 2000) (Figures 3A, S1B–S1E, and S3; Table S1C). Zooid brains consist of a cerebral ganglion, possessing a cortex of neuronal somata and an inner medulla of neurites that are connected to several mixed nerves. It is connected to a neural gland, a sac-like structure that opens anteriorly into the pharynx, and a dorsal organ (Figures 1H, 3B, S1K, S1L, and S3; Table S1C) (Burighel and Cloney, 1997; Manni and Pennati, 2015).

The origin of the nervous system in mammals begins with the induction of the neural ectoderm shortly before gastrulation (Spemann and Mangold, 2001), and it was tracked to the 32-cell stage (morula) in the solitary tunicate, *Ciona intestinalis* (Nishida and Stach, 2014). Recently, Cao et al. (2019) used single-cell sequencing to construct cell-lineage maps and provisional gene networks for 41 neural subtypes that comprise the *C. intestinalis* larval nervous system.

The first enrichment of nervous system genes in *B. schlosseri* lies between eight cells (E1.3) and blastula (E1.5) (Figure 3B). The enrichment profile stabilizes during the gastrula, neurula, and early tailbud stages, when the neural plate forms, and it develops the main components of the larval nervous system (Figures 3A and S3A–S3H; Table S1C). The second enrichment appears during the wrap stages (E4–E6), when the development of the larval and oozooid brain becomes evident (Figures 3A and S3A–S3H; Table S1C). Out of 28 putative TFs that are activated at E1.3, nine are associated with neural crest, brain, and nervous system development, including *Pou3f3*, *Dix1*, *Lmx1a*, *Sox6*, *PA2G4*, *Zmat4*, *Zfp318*, *Cebpz*, and *Aedbp1* (Table S3B). Their expression most likely induces the neural ectoderm in the *B. schlosseri* embryos at E1.3. During the wrap stages (E4–E7), 78 dynamically expressed genes are associated with the *B. schlosseri* nervous system (Table S3A). Of these, eight genes, including *TIAM2*, *DLG5*, and *MDGA1*, are known to be involved in regulating cell proliferation, neurite growth, migration, and axon guidance. The expression of these genes is shown in Klee plots (Figures 3E and 3F). Their expression increased during key nervous system developmental stages in both pathways. During metamorphosis, when the larval nervous system is resorbed while the oozooid cerebral ganglion remains, the gene signature stabilizes (Figures S3E–S3H).

During embryogenesis, the oozooid cerebral ganglion forms from a tubular structure, the neurohypophyseal duct, that derives from the anterior neural plate (Table S1C). The duct, which represents the rudiment of both cerebral ganglion and neural gland, is initially connected to the ganglionic vesicle, but later it loses this original connection and grows forward to open into the anterior pharynx. The pharynx aperture forms the ciliated duct of the neural gland, whereas its posterior forms the body of the neural gland and the dorsal organ (Manni and Pennati, 2015). Meanwhile, the neurohypophyseal duct wall proliferates pioneer nerve cells, which coalesce to organize the cerebral ganglion. This brain is retained after metamorphosis in the oozooid (Figure 3C).

During blastogenesis, the neural complex rudiment forms from a thickening of the dorsal area of the secondary bud (b5–b6) (Figures S3I–S3J). This develops into the dorsal tube, which grows forward and fuses with the anterior pharyngeal wall during the transition into the primary bud (b→B). At the same time, pioneer nerve cells appear on the dorsal tube that differentiate into the neural gland and the posterior dorsal organ. In the early primary bud (B1–B2) the cerebral ganglion and the neural gland are connected, pioneer nerve cells proliferate, and nerves appear (Figures S3K–S3M). When the primary bud is about to replace the resorbing zooid (B→A), a massive reduction in the number of nerves occurs and the neural complex reaches its typical adult configuration (Figure S3N) (Zaniolo et al., 2002). The whole complex is progressively destroyed during TO (Figures S3O and S3P), when apoptosis and programmed cell removal lead to engulfment of the brain cells.

A high degree of concordance between known differentiation timelines, morphological observations, and tissue-associated transcriptional profiles are observed in blastogenesis (Figure 3D). In particular, the enrichment of nervous system-associated genes reflects the nervous system's development and morphogenesis processes. For example, the reduction of nerves observed in the primary bud during generation changes (B→A), which is

accompanied with inhibition of 48 TFs associated with the mammalian nervous system and brain development, including *SOX9*, *OTX2*, *FOXD3*, and *SMAD1* (Table S3D).

Taken together, *B. schlosseri* offers a unique system to study neurogenesis. During chordate embryonic development a larval brain is formed with functions required for a swimming larva to find a settlement site, after which the larval brain is resorbed. The embryonic phase also develops a second brain, connected with the larval brain, but which persists after metamorphosis. This brain is regenerated during every blastogenic cycle, perhaps analogous with mammalian neurogenesis, from persisting CNS stem cells. The similarities and differences between the two molecular pathways suggest common and different regulation between development and regeneration (Table S5B).

Origin of the hematopoietic system and its niche

In mammalian blood, mature lineages, including erythrocytes, platelets, and innate and adaptive immune cells, are generated from HSCs (Spangrude et al., 1988). Hematopoiesis and the factors that regulate HSC self-renewal are highly conserved among vertebrates (Jagannathan-Bogdan and Zon, 2013). Recently, we isolated prospective HSCs and progenitor cells in *B. schlosseri* and identified the endostyle as their niche (Rosental et al., 2018). The endostyle is a complex tissue that is found in tunicates, cephalochordates, and in the larvae of lampreys (Figures 4A, 4D, and 4E) (Burighel and Cloney, 1997; Cañestro et al., 2008; Ogasawara et al., 1999; Rinkevich et al., 2013; Rosental et al., 2018; Voskoboynik et al., 2008). During embryogenesis, blood cells appear gradually, concurrent with the formation of the blood ampullae (E4), forming the first circulatory system (Table S2C; Figures S4A–S4G) (Burighel et al., 1983; Milanesi and Burighel, 1978; Brunetti and Burighel, 1969). In early wrap (E4) lymphocyte-like cells (hemoblasts) as well as morula cells are detected (Figures S4A and S4B; Table S1C). By mid-late wrap (E6), phagocytic cells (hyaline amoebocytes) and pigment cells are detected (Figures S4C–S4E), and during metamorphosis, macrophage-like cells appear (E7–E8) (Figure S4F). Nephrocytes and pigmented cells differentiate in the oozooid (E9) (Figure S4G). The blood cells morphologically present in the oozooid constitute all blood cells that will be later observed in adult colonies (Ballarin and Cima, 2005; Rosental et al., 2018).

There is a large degree of correlation between the morphological observations and the enrichment of *B. schlosseri* HSC-associated genes between E4 and E5 (Figures 4B and 4C). In the solitary tunicate *Ciona*, hemocytes are recognized only after metamorphosis, but their lineage has been traced to the 64-cell embryos (cleavage period) (Kawaminani and Nishida, 1997), corresponding to E1.4–E1.5 in *B. schlosseri*. The HSC signature is high early in development (E1.1–E1.4), decreases during E1.5–E3, increases again during the wrap stages (E4–E6), and then stabilizes after the larval stage (Figure 4C). The expression levels of a subset of these genes, including *ALOX5*, *SELE*, and *SELP* homologs, have about a 1,000-fold higher expression in late wrap than early wrap. Morphologically, this increase coincides with the appearance of hemoblasts in the early wrap (E4) (inset in Figure 4C). The cellular characterization was validated by flow cytometry (Figure 4B).

During metamorphosis, the oozooid inherits its hemocytes from the larva. Hemocytes circulate within zooid cavities (sinuses) and the colonial circulatory system. In the secondary

bud, they are recognizable in the first sinus at stage b4. The HSC enrichment pattern shows a relatively steady signature along blastogenesis, with lower expression in primary and secondary buds on days 3 and 4 (B3b3–B4b4) and in zooids during TO (Figure 4F). As the number of HSCs and their progenitors increase in the primary buds and zooids during B5 to A5, the enrichment profile increases as well. Toward the TO stage the HSC signature decreases (Figure 4F).

During blastogenesis, stem cells, including HSCs, reside and proliferate in the anterior ventral side of the endostyle (Figures S4K–S4O) (Rosental et al., 2018; Voskoboynik et al., 2008; Figures S4N, S4Q, and S4R). The endostyle extends medially at the ventral face of the zooid branchial sac along its anterior posterior axis consisting of eight distinct symmetric anatomical zones (Figure S4N). It is immersed in blood flow through sinuses (Burighel and Brunetti, 1971) (Figures S4Q and S4R). The enrichment of *B. schlosseri* endostyle-associated genes during embryogenesis revealed an increase in their expression from E1.1 to E1.4 (Figure 4C), including 239 genes with human homologs expressed in hematopoietic bone marrow. In embryogenesis, the endostyle is clearly recognized during mid-wrap (E5) (Figures 4A, 4E, and S4H–S4J), coincident with the increase of associated genes (E4–E6), which succeeded those of HSCs (E4) (Figures 4B and 4C). However, in blastogenesis, the endostyle gene enrichment fluctuates dramatically (Figure 4F). The first wave of enrichment (b5–b6 in Figure 4F) is associated with the appearance of the endostyle (Table S1C; Figures 4D, 4E, and S4K). The formation of the eight zones (Figures 4D, 4E, S4M, and S4N) coincides with the second wave of enrichment (B5–B6, A1) (Figure 4F). During TO when the endostyle is destroyed (Figure S4O), the enrichment drops off (Figure 4F). In both embryogenesis and blastogenesis, the endostyle follows the same developmental stages, creating a highly similar anatomy with eight zones (Figure 4E; Table S1C) and expressing TFs essential to the early development, including FOXD3, PPARG, ATF4, PROX1, and PPARD (Table S3).

Origin of reproductive tissues

The germline is made up of a highly protected and strictly regulated group of cells that transmit genetic information to the next generation. In vertebrates, the germline originates as a very small founding population, segregated from somatic cells early in development (Anderson et al., 1999; Dixon, 1994; Soriano and Jaenisch, 1986; Ueno et al., 2009; Weismann, 1892). *B. schlosseri* is hermaphroditic and gonads are detectable only after several blastogenic cycles (Kawamura et al., 2011). In natural chimeras, GSCs migrate via the colony vasculature and home to its niches and the developing buds where they compete for germline lineages (Laird et al., 2005; Rinkevich et al., 2013; Rosental et al., 2018; Stoner and Weissman, 1996; Stoner et al., 1999; Weissman, 2015). We expect a gene signal from GSCs in both embryos and in colonies before they sexually mature.

Our candidate GSC enrichment profile suggests that in the embryo they are established at morula (E1.4) and expand as the embryo grows (Figures 5D and 5E). There is a slow increase in GSC signals during early cleavage (E1–E3); at these stages, candidate germ precursor cells expressing vasa were identified in *B. schlosseri* (Brown et al., 2009). The enrichment peak in the morula (E1.4) aligns with high expression of *NR6A1* (also known as

GCNF), a TF involved in germ cell development and neurogenesis, and it corresponds to the emergence of GSCs at the 4- to 16-cell stage in mice (Anderson et al., 1999; Dixon, 1994; Soriano and Jaenisch, 1986). In other tunicates, germ cells are first recognized at the 64-cell stage in *Halocynthia roretzi* (Kawamura et al., 2011), and the gastrula (stage 13) in *Ciona* (Shirae-Kurabayashi et al., 2006). The increased enrichment signature after E6 is reflected in flow cytometry measurements (Figure 5D). In embryogenesis (Figure 5E), the germ and testis signatures are aligned until the late wrap stage (E6). This is expected, as the two share almost 30% of their enriched genes (Figures 5E and 5F; Table S3E). The oozooid is not sexually mature, so while general stem-associated genes continue to be expressed (germ signal), those for the testis decrease to baseline.

Adult *B. schlosseri* forms male and female organs on both lateral body walls. The testes and eggs develop during reproductive seasons. We analyzed the male gonads, which in the secondary bud (b3) are a loose mass of primordial germ cells and somatic cells close to the inner vesicle wall (Table S1C; Figures 5A, 5B, and S5A). Germ cells expressing vasa were detected at this stage (Rosner et al., 2009). As soon as the testis wall is formed (b5), it becomes a compact mass with spermatogonia undergoing meiosis. This wall separates the testis from the forming female gonad (when present) and subdivides into lobes (testicular follicles), in which an initial lumen can be seen (Figures S5B and S5C). In primary buds (Figures S5D and S5E), the testis progressively enlarges and completes its development. The mature testis in zooids possesses four to five lobes displaying a gradient of sperm maturation: spermatogonia are located at lobe periphery, followed by primary spermatocytes, secondary spermatocytes, spermatids, and fully mature spermatozoa at the lobe center (Figures S5F–S5H); sperm are released at stage A3.

Germ and testis enrichment profiles both show sharp and strong enrichment in the early buds (b1–b2/B1–B2) (Figure 5F). This is the time immediately before gonad establishment in secondary buds (b3) and the emergence of testis gross anatomy in primary buds (B3). A second sharp increase in testis gene expression enrichment characterizes the late primary bud stages involving spermatid maturation, and in adult zooids (A3–A4), corresponding to the last phases of testes maturation preceding spawning. GSCs, in adults, constitute a pool of cells able to circulate in the colony vasculature, reside in cell islands (Figures S4Q–S4T), and colonize the gonad niches in the following blastogenic generations, as reflected by the very high enrichment at this time (b1–b2/B1–B2) (Rinkevich et al., 2013; Sabbadin and Zaniolo, 1979; Stoner and Weissman, 1996; Stoner et al., 1999).

Many markers for primordial germ cells are observed during early embryogenesis and blastogenesis, including alkaline phosphatase (Chiquoine, 1954; Ginsburg et al., 1990), SSEA-1/FUT4 (Marani et al., 1986), Oct3/4/POU (Rosner et al., 2009), Blimp-1/PRDM (Saitou et al., 2005), Piwi (Cox et al., 2000), and vasa/DDX4 (Castrillon et al., 2000; Raz, 2000). These shared signatures along these two developmental pathways form a link between the germline embryonic and adult stem cells (Table S3F).

Tissue-specific transcriptional timings are shared in both developmental pathways

An open question is to what extent organ development in each pathway shares molecular signatures. To answer this, we systematically identified the developmentally dynamic tissue-

associated genes that were enriched before and after different times in each pathway and compared the enrichment of those genes in the other pathway (Figure S6). This identified both the time of early to late gene transitions as well as the correspondence of organogenesis times (Figures 6 and S6; Table S6). For example, in blastogenesis there is a clear early/late pattern of HSC-associated genes that cross during the B→A stage (Figure 6A; Table S6). The same pattern for these genes is observed in embryogenesis at E4–E5 (Figure 6B; Table S6). When applied to all tissue/cell types examined in this study, this analysis revealed both the conservation of early/late tissue-specific gene expression (molecular development) and the shared chronology of tissue emergence (global development) (Figure 6C). The exception is the nervous system, which emerges precociously in the embryo compared to the zooid. This may be due to the development of the notochord and larval nervous system that are unique embryonic traits.

These early and late gene expression patterns can help find the genes associated with the stem versus differentiated cell state during organogenesis (Table S6). Our findings suggest that cellular trajectory is defined early in development and demonstrate that blastogenic tissue-specific stem cells and their embryonic precursor cells share similar molecular dynamics.

Evolution of TFs and the regulation of chordate development

All members of *Chordata* (cephalochordates, tunicates, and vertebrates) develop a defined body plan during embryogenesis. Through comparing members of this phylum, we can track the evolution of chordate development, with each member show-casing different applications and expressions of chordate features that, when combined, aid in understanding the evolution of early vertebrates. Colonial tunicates lose most of their chordate characteristics when they metamorphose into an adult form and are the only chordates to possess sexual and asexual developmental programs (e.g., embryogenesis and blastogenesis). These two traits make *B. schlosseri* especially relevant for evolutionary developmental biology (evo-devo) chordate studies. To place *B. schlosseri* development in the context of other chordates, we compared its developmentally dynamic genes with those in the cephalochordate amphioxus (*Branchiostoma lanceolatum*) and the vertebrate zebrafish (*Danio rerio*) using publicly available data (Marlétaz et al., 2018) (Figures 7 and S7; Table S7). For these other species, the developmentally dynamic genes were calculated using our methods (see STAR methods; Methods S1; Tables S7A and S7B). The embryogenesis timelines comparison between amphioxus and zebrafish supports the location of the phylotypic period, the period with maximal molecular similarity (Duboule, 1994; Hu et al., 2017; Irie and Kuratani, 2011), as found previously (Marlétaz et al., 2018).

By comparing how the overall molecular expressions for all of these developmental programs are related, we discovered where the molecular pathways converge and diverge. For each comparison between species, we calculated the correlation of the binary gene matrix at each developmental stage and determined periods of similar and distinct gene expression in an unbiased manner. First, we estimated the correlation values expected from interspecies comparison by using a null model based on shuffling gene expression within each time point (so the total number of activated genes remained constant, but the identity of

the genes was random). Null correlations between *B. schlosseri* and amphioxus were between —0.01 and 0.07, and between *B. schlosseri* and zebrafish ±0.04 (Figure S7C, lower), with values outside these indicating periods that are more or less similar than would be expected randomly. When all conserved genes were compared (Figure S7B), the developmental trajectories showed little to no significant correlation when compared with *B. schlosseri* embryogenesis, but they did when compared with blastogenesis.

We repeated the comparison of all developmental programs with a focus on evolutionarily conserved putative TFs (Figure S7A), with significant correlation values identified as those above ±0.2 (Figure S7C, upper). The TFs enrichment list was compiled by Lambert et al. (2018), which includes about 1,600 known and putative human TFs. Out of this list, 924 putative TFs maintained sequence homology in both humans and at least one of the investigated chordates species (Tables S7C and S7D).

B. schlosseri embryogenesis and blastogenesis programs share putative TFs with embryogenesis of other chordates, and the maximum correlation detected was 0.3, indicating dissimilar molecular programs between these species (Figures 7A, 7B, S7A, and S7B; Tables S7C and S7D). Indeed, among the 924 putative TFs that are shared between the three species and human, many of them are either (1) uniquely expressed in one of the species but not the others (e.g., 116, 169, and 235 TFs uniquely expressed in *Botryllus*, amphioxus, and zebrafish, respectively), (2) expressed in two out of the three species (118, 115, and 53 TFs are shared between *Botryllus* and amphioxus, amphioxus and zebrafish, or *Botryllus* and zebrafish, respectively), or (3) expressed in all (118 putative TFs; Table S7D). This suggests that the common ancestor of tunicates, cephalochordates, and vertebrates had homology to at least 57% of the human TF repertoire. Notably this list of shared putative TFs depicts representatives from most human TF family members, with the main difference being the multiplicity within specific families (e.g., 500 zinc finger [ZNF] gene family members in humans compared to 178 ZNF members cumulatively found in the three chordates species; Table S7D). These results support the hypothesis that at least two genome duplications occurred in the transition from invertebrate to vertebrate (Ohno, 1970; Simakov et al., 2020), and further point to evolutionary conserved putative TFs families that went through multiplication (Table S7D).

When the enriched TFs showed correlation, the estimated equivalence of developmental trajectories tended to have consistent and continuous downward trends (Figures 7And 7B, a S7A). Early *B. schlosseri* embryogenesis (E1.2–E4) resembles that of early embryogenesis in other chordates: amphioxus egg, 10 h post-fertilization (hpf); and zebrafish, 2–12 hpf (Figure 7A and S7). This correspondence in early developmental stages can be credited to the establishment of the common bauplan in the representatives of the three subphyla. Indeed, focusing on periods with conserved TF expression revealed that during early chordate development we observed high expression of TFs that are associated with regulation of cell cycle (FoxM1), stem cell pluripotency (TBX3), and axial patterning (DLX1) (Figure 7C). The later stages and final product of embryogenesis (E5–E9) do not align with the later stages of amphioxus and zebrafish embryogenesis. This difference is likely due to the process that *B. schlosseri* larvae undergo as they prepare to metamorphose into a zooid, a process that the zebrafish and amphioxus do not undertake (Figures 7A and

S7A). Blastogenesis, alternatively, extends across later time points, with the strongest resemblance appearing when we compare the later periods (A1 to TO) to the later stages of amphioxus development (Figure 7B). We observed similar patterns between *Botryllus* and zebrafish (Figure S7A), which could be associated with the completion of organ formation at these stages, as evidenced by the high level of TFs mainly associated with metabolism (e.g., HNF1A), adipogenesis (e.g., HAR), and cell fate determination (e.g., DACH1) (Tables S7C and S7D; Figure 7C). The higher correlation values that occur between amphioxus and *Botryllus* compared to zebrafish are likely caused by the unique endostyle tissue amphioxus and *Botryllus* share.

Our data support former studies that identified TFs as evolutionarily conserved regulators of development (Davidson et al., 2002; Farley et al., 2015; Krumlauf, 1994; Prummel et al., 2019). Given that comparison of all genes between species showed low correlation, we propose that while the expression and timing of TFs is conserved in development, the genes activated/repressed downstream are less evolutionarily constrained. Comparing the pathways associated with the shared and unique putative TFs among *Botryllus*, amphioxus, and zebrafish, we identified shared and specific enrichment paths underlying the emergence and early diversification of vertebrates (Table S7E). The pathways enriched in each of these species reflect their life history and point to specific traits. For example, pathways that play an important role in hematopoiesis and heart and vascular development are enriched in *Botryllus*, circadian rhythm paths are enriched in amphioxus, and pathways associated with the adaptive immune system are uniquely expressed in zebrafish. Alternatively, pathways that are shared by all species point to the conserved traits essential to chordate development.

In conclusion, the *B. schlosseri* morphogenetic atlas of sexual and asexual development provides an essential new resource for studying the morphogenesis, genes, and regulatory logic that control stem cell-mediated developmental pathways. It deals with one of the great challenges in evolutionary biology, which is to understand how differences in developmental gene expression within the same species and between species underlie phenotypes. Through this research, we have opened a venue to explore vertebrate development and better understand human stem cells and TF evolution.

STAR★METHODS

RESOURCE AVAILABILITY

Lead contact—Further information and requests for resources and reagents should be directed to and will be fulfilled by the lead contact, Ayelet Voskoboynik (ayeletv@stanford.edu).

Materials availability—This study did not generate new unique reagents.

Data and code availability—The published article includes the code generated during this study (see Methods S1 and S2).

The sequencing data generated during this study are available on the NCBI Sequence Read Archive under accession: PRJNA579844. Values of transcripts counts and gene expression analysis results are shown in Tables S2 and S3.

A detailed description of *B. schlosseri* embryogenesis, blastogenesis. and Organ development in both pathways are shown in Table S1.

Three dimensional reconstructions can be found on morphonet browser using the following link: https://morphonet.org. Login: Botryllus3D Password: oozooid

EXPERIMENTAL MODEL AND SUBJECT DETAILS

Specimens of *Botryllus schlosseri* (family *Botryllidae*, order Stolidobranchiata) used in this study were collected from both the lagoon of Venice (IT) and Monterey Bay (CA). The colonies from Venice lagoon were used for histological analyses, 3D reconstructions and the Transmission Electron Microscopy (TEM). The colonies from Monterey Bay were used to sample specimens for confocal and two photon microscopy, RNA sequencing, and FACS analysis and to study the *ex-vivo* embryogenesis timeline.

METHOD DETAILS

Mariculture—Mariculture procedures have been described previously (Boyd et al., 1986). Briefly, wild-type *Botryllus schlosseri* colonies were tied to 3×5-cm glass slides and placed 5cm opposite another glass slide in a slide rack. The slide rack was placed into an aquarium, and within a few days the tadpoles hatched, swam to the settlement slide, and metamorphosed into the adult body plan (oozooid). Single oozooids are then transferred to individual slides and grown at 18–20°C. Colonies were fed daily using a marine invertebrate diet prepared in the lab as follows: Heat 150 mL dH2O to approx. 80°C. Pour 100ml in a blender container and add 1½ tablespoons whole egg powder,1 tablespoon nutritional yeast, 1½ teaspoon garbanzo bean powder, ½ teaspoon spinach powder and ¼ teaspoon lecithin powder. Blend until thoroughly mixed. Pour into a microwavable glass container and heat the mixture in a microwave for 20 s @ power level 4. Remove from the microwave and swirl. Repeat 4–6 times until lighter in color and thickened. Do not allow it to curdle. Add an additional 50ml warm dH2O. Pour back into the blender and mix until smooth. Place in an ice water bath until cold. Store at 4°C. Dilute 1:10 with fsw for animal use.

Samples were collected at different blastogenesis and embryogenesis developmental stages. Staging methods were based on (Sabbadin, (1955); Manni et al., 2014) staging method for blastogenesis, and the anatomical and developmental ontology of *Ciona intestinalis* (https://www.aniseed.cnrs.fr/) for early stages of embryogenesis.

For both developmental pathways, a numerical staging method that refers to the day of development for embryo (E), secondary bud (b), primary bud (B) and adult zooid (A) was developed (Table S1; Figures 1A, 1B, and 2A), simplifying the comparison between *B. schlosseri*'s two developmental pathways and embryogenesis in other chordate species. In the numerical methods developed, E indicates embryogenesis and the first number is the number of days typically elapsed during development at 18–20°C. The second digit (where

present) counts the stages present in a single day of development. For the blastogenic pathway each generation is represented with a letter: secondary buds (b), primary buds (B) and adult zooids (A) with numbers indicating the days of development of that generation. Transitions between generations are marked as b→ B, B→ A, TO (take over).

***Ex vivo* embryogenesis and embryos collection for sequencing—**Wild parental colonies were dissected under a Wild Stereomicroscope, and embryos were collected and separated into 35mm Petri dishes according to stage. Embryos were kept in filtered seawater at room temperature and their development was tracked by timelapse microscopy using a BZ-9000 Keyence microscope (Video S1).

For RNaseq library prep staged embryos were frozen in liquid nitrogen, and held at −80.

Sample collection for sequencing—Tissue samples were collected from *Botryllus schlosseri* colonies raised in the Hopkins Marine Station Mariculture Facility. Animals were isolated without food for 20 hours prior to dissection. Tissues were obtained by microdissection, frozen in liquid nitrogen, and held at −80 prior to library preparation. Tissues and organs (Figure 1C) were sampled from zooids on stage A1–2. In embryogenesis, specimens were taken from 15 different developmental stages across 7 days, (Figure 1A; n = 44). In blastogenesis, secondary buds, primary buds, combinations of both buds and the adult zooids were taken from 12 developmental stages over a period of 7 days (Figure 1B; n = 29). To identify tissue/cell specific signatures, we sequenced different tissues, organs and cell populations taken from zooids including: dissected testes, endostyles and brains (cerebral ganglion, dorsal organ, and neural gland); and blood vessels embedded within the tunic (Figure 1F; Figure S2; n = 27).

Library preparation—RNA was prepared from frozen samples using Zymo Research Quick RNA MIcro Prep Kit # R1050, and cleaned using Zymo Research RNA Clean and Concentrator, #R1015. Samples were analyzed on an Agilent QC 2100 Bioanalyzer to determine quality prior to library preparation. cDNA was prepared used the Nugen Ovation RNA Sequencing System V2, #7102 and cleaned using the QIAGEN QIAquick PCR purification kit, #28104, as recommended in the protocol and analyzed on the Agilent QC Bioanalyzer. If needed, samples were size-selected using Zymo Research Select-A-Size DNA Clean and Concentrator #D4080 prior to barcoding. Final library was prepared using NEB NEBNext Ultra II DNA Library Prep Kit #27645 and barcoded using NEBNext Multiplex Oligos for Illumina #E6609S. All magnetic bead purification was accomplished using BullDogBio CleanNGS RNA and DNA Spri Beads #CNGS005. Samples were then analyzed on the Agilent QC 2100 Bioanalyzer to determine the concentration of each sample prior to determine dilution prior to sequencing. On average, 12 million 2×150 bp reads (Illumina Nextseq 500) were sequenced for each library.

Gene counts—Following sequencing, reads were processed using a Snakemake (Köster and Rahmann, 2012) pipeline: they were trimmed to remove low quality bases and primers, merged if the reads from both ends overlapped, and aligned to a database of *B. schlosseri* transcripts using bwa (mem algorithm), with likely PCR duplicates removed and then read

counts determined for each transcript, resulting in 3 count tables: S2A-embryogenesis, S2B-blastogenesis, and S2C-tissue specific.

Gene orthology—Gene orthology is based on sequence similarities between the *B. schlosseri* gene models and human and mouse gene annotations (BLAST score smaller than 10^{-10} as described in the *B. schlosseri* genome paper; Voskoboynik et al., 2013a), and explained in the main text that all discussion regarding genes and putative transcription factors (TFs) are based on sequence similarities alone.

Identification of developmentally dynamic genes and formation of binary tables—To quantify gene expression patterns across time in each pathway, the following method to identify developmentally dynamic (i.e., changing) genes was adopted:

- Two subsets of times (identified here as *A* and *B*) in a pathway were selected (either sets of contiguous times, as in Figure 1C, upper right) or allowing for multiple sets of these (*A1*, *B1*, *A2*, *B2*…) to account for the multiple generations of organism present in the blastogenic cycle.
- Samples associated with *A* and *B* times were each grouped together and differentially expressed genes were found using edgeR (Robinson et al., 2010).
- For each gene, all such comparisons for which statistically significant differences (FDR < 0.05) were recorded.
- The time signature (modeled as a series of ‘‘+’’ and ‘‘-’’s for all the time points) that had the greatest agreement with the observed set of differential calls for a given gene was selected and this signature binarized, with 1 indicating ‘‘high’’ expression and 0 indicating ‘‘low’’ or zero expression producing a gene-time expression matrix for each gene along the developmental pathway (Tables S3A, S3B, S7A, and S7B).

See Methods S1 for detailed Python code used.

Gene enrichment plots—To generate a quantitative understanding of how enriched/expressed a set of genes is at different times in the developmental pathways the following was done:

1. At each time the proportion of genes in a gene set that are active (indicated by a 1 in the gene-time expression matrix defined above) is calculated. This gives a value between 0 (no genes in common) and 1 (all genes in the gene set are active at that time).
2. A baseline expectation of the proportion of overlapping genes is calculated using a hypergeometric model where the same number of genes as in the selected gene set would be randomly selected from the gene-time expression matrix.
3. In addition, the 50% and 99% confidence intervals of proportion of shared genes (‘enrichment’) from the hypergeometric are calculated.

4. Then the baseline is subtracted from the values calculated in (1), with the confidence intervals from (3) also subtracted to show the expected range of values and how far the actual enrichment result differs from a null result.

See Methods S2 for detailed Python code used.

Tissue enriched genes—For the nervous system, endostyle, testis and ampullae, differentially expressed genes were found on all pairwise comparisons and then gene sets picked from unions and intersections of these comparisons (see Figure S2A; Table S2C). Existing gene lists associated with HSCs and candidate germ cells (Rosental et al., 2018), were also used.

Klee plots—Heatmaps are often used to present gene expression data for many genes and many samples simultaneously. Another approach to presenting this data would be to produce summary statistics (such as the mean) for each stage (i.e., a grouping of samples) and present this as a heatmap or line plot. In order to keep the comprehensiveness of a heatmap while grouping samples belonging to the same stage together we developed a new heatmap-like plot we have named ‘‘Klee’’ plots (named after Swiss artist Paul Klee whose works include irregular colored rectangles).

In a Klee plot, each row is a gene and each column is a grouping of samples (e.g., specific developmental stage). But within a given row/column region there are rectangles that show the expression of individual samples. The outside of entries is the mean value over samples for a given gene and time, providing a summary statistic of the data.

Species comparison—Tunicates, cephalochordates, and vertebrates constitute the three extant groups of chordate animals. To compare developmental dynamics between other chordates, public raw sequence data was downloaded from NCBI for amphioxus (cephalochordates) and zebrafish (vertebrates) (Marlétaz et al., 2018). These were processed using a Snakemake pipeline in a similar way to the *B. schlosseri* sample. Reads were trimmed, aligned to UniVec core using bowtie2 and aligned reads removed. Cleaned reads were aligned to the appropriate reference databases using STAR (Dobin et al., 2013) and genes counted using htseq (Anders et al., 2015) (intersection-nonempty mode, secondary and supplementary alignments ignored) against reference GTF files. From count tables developmentally dynamic genes were determined in the same manner as for *B. schlosseri*.

To compare different times in different organisms, rows (gene IDs) were grouped by gene name according to amphioxus (Marlétaz et al., 2018) and zebrafish (ENSEMBL, release 100) genome annotations. If multiple gene IDs had the same name, they were collapsed into a single object with all positive values (‘‘1’’) being kept. This in general was done for all times in different developmental pathways and common gene names kept. Optionally the list of common genes was also restricted to those that shared names with a list of human transcription factors (Lambert et al., 2018). The two binary gene enrichment vectors are then compared and the correlation distance computed.

Histology—Embryos and buds were fixed for 2 hours in 1.5% glutaraldehyde in 0.2M sodium cacodylate and 1.6% NaCl buffer. After 3 washes in 0.2 M sodium cacodylate and

1.6% NaCl buffer, samples were post-fixed for 1 1/2 hours in 1% OsO4 in 0.2M cacodylate buffer at 4°C. Samples were dehydrated and then soaked in Epon and propylene solution at 37°C, 45°C, and 60°C. They were then embedded in resin, oriented and sectioned using a Leica ultramicrotome. Sections, 1 μm thick, were stained with toluidine blue.

Electron microscopy—Colonies were anesthetized with MS222 for 5–10 minutes; then, selected fragments of colonies, cut with a small blade, were fixed in 1.7% glutaraldehyde buffered with 0.2M sodium cacodylate plus 1.6% NaCl, pH 7.4. After washing in buffer and post-fixation in 1% OsO4 in 0.2 M cacodylate buffer, specimens were dehydrated and embedded in epoxy resin (Sigma-Aldrich). Semithin sections were stained with 1% toluidine blue in borax. Ultrathin sections (80 nm thick) were stained with uranyl acetate and lead citrate to provide contrast. Photomicrographs were taken with a FEI Tecnai G12 electron microscope operating at 100 kV. Images were captured with a Veleta (Olympus Soft Imaging System) digital camera.

3D reconstruction—An oozooid (E9), a bud and secondary bud (B1+b1) and a larva in early metamorphosis (E7-E8), were embedded in resin as previously described and serially transversely cut using a Histo Jumbo Knife (Diatome). Sections, 1 μm thick, were arranged in chains of about 20 sections each and stained with toluidine blue. All the sections were then photographed with Leica DMR optical microscope. Images were aligned using Adobe Photoshop CS on a Windows 7 computer. Based on the resulting stack of images, 3D models of the anatomy of all organ systems were created in Amira software (Thermofisher scientific). Reconstructions were made in 3D of a larva in early metamorphosis (E7-E8), an oozooid (E9), and a primary bud and secondary bud (B1+b1) using 426, 853, and 375 sections respectively. Their organs and tissues can be visualized using the MorphoNet browser (Figures 1G–1I; Figure S1) (Leggio et al., 2019).

Confocal imaging—Embryos, larvae, secondary buds, primary buds and zooids were dissected under a Wild Stereomicroscope, collected and separated into 35μm Petri dishes according to stage. Following several washes in sterile filtered seawater samples were fixed for 30 min at room temperature with 4% paraformaldehyde in MOPS buffer (0.1M 3-(N-Morpholino) propane sulfonic acid), adjusted to pH 7.5 and washed 2 times in 1xPBT buffer (Phosphate-buffered saline with 0.1% triton-100). Fixed samples were stained for 30 min in 1/1000 diluted cell mask orange for staining cytoplasm. After 3 washes with PBT, Alexa Phalloidin 546 was used for actin staining overnight at 4 C°. Samples were made transparent by dehydrating them with a series of solutions of 2–propanol in PBT and then with BABB (benzyl alcohol (Sigma B-1042)/ benzyl benzoate (Sigma B-6630) 1:2 ratio). In case of nucleus staining, embryos were stained with DAPI (Vector Laboratories) instead of BABB and mounted in Vectashield mounting medium. Stained samples were observed using confocal laser microscopy (Olympus fv1000) under ×10 - ×40 oil objective lens. 3D images were reconstructed from stack images (interval 1 to 3 μm) using Imaris software.

Flow cytometry—Embryos were taken at different stages and cell suspension was isolated as described (Rosental et al., 2018). Briefly, *B. schlosseri* embryos were meshed and filtered through a 40 μm mesh using a sterile 1 mL syringe pump. Cells were washed and collected

in staining media: 3.3x PBS, 2% FCS and 10 μm HEPES. Cells were labeled Propidium Iodide (PI), to differentiate live versus dead cells, and with Alkaline Phosphatase (AP) Live Stain (Life Technologies A14353) 1ml, for labeling of candidate stem cell populations (Rosental et al., 2018). After gating on negative PI cells (using two dimensional plots due to natural fluorescence of *B. schlosseri* cells), the cells were analyzed on positive AP and - forward scatter (FSC) and granularity - side scatter (SSC) panel on log scale using BD ACCURI-C6. All experiments were done on pooled embryos (at least 6 individuals) for each measurement. Analysis of flow cytometry data was accomplished using FlowJo V10 (FlowJo).

QUANTIFICATION AND STATISTICAL ANALYSIS

Detailed description of number of samples used for sequencing is included in the main text, figures, and methods.

No statistical methods were used to predetermine sample size.

The experiments were not randomized and the investigators were not blinded to allocations during experiments and outcome assessment.

Statistical method of computation including the statistical methods used to find differentially expressed genes and the hypergeometric model used to show the expected range of values and how far the actual results differs from a null result are described in details in the methods, figures and main text.

Supplementary Material

Refer to Web version on PubMed Central for supplementary material.

ACKNOWLEDGMENTS

We thank C. Lowe, T. Raveh, C. Patton, R. Voskoboynik, A. Olson, Y. Voskoboynik, P. Bump, J. Thompson, J. Lee, B. Compton, N. Myers, and T. Naik for technical advice and help and E. Faure for hosting 3D models on MorphoNet.org. This study was supported by NIH grants R56AI089968, R01AG037968, and RO1GM100315 (to I.L.W., S.R.Q., and A.V.); NIH grant R21AG062948 and the Chan Zuckerberg Investigator Program (to I.L.W. and A.V.); the Virginia and D.K. Ludwig Fund for Cancer Research, a grant from the Siebel Stem Cell Institute, and a Stinehart-Reed Grant (to I.L.W.); an NIH shared equipment grant (1S10OD025091–01); PRIN-Prot. 2015NSFHXF (to L.M.); a Larry L. Hillblom Postdoctoral Fellowship, Stanford School of Medicine Dean's Postdoctoral Fellowship, Aldo Gini foundation Fellowship, and an Iniziative di Cooperazione Universitaria 2017 Fellowship of the University of Padova (to C.A.); and HFSP grant LT000591→2014-L, NIH grant T32 HL120824–03, ISF grant 1416→19, and HFSP grant RGY0085/2019 (to B.R.).

REFERENCES

Alié A, Hiebert LS, Scelzo M, and Tiozzo S (2020). The eventful history of nonembryonic development in tunicates. J. Exp. Zoolog. B Mol. Dev. Evol Published online March 18, 2020. 10.1002/jez.b.22940.

Anders S, Pyl PT, and Huber W (2015). HTSeq–a Python framework to work with high-throughput sequencing data. Bioinformatics 31, 166–169. [PubMed: 25260700]

Anderson R, Schaible K, Heasman J, and Wylie C (1999). Expression of the homophilic adhesion molecule, Ep-CAM, in the mammalian germ line. J. Reprod. Fertil 116, 379–384. [PubMed: 10615264]

Ballarin L, and Cima F (2005). Cytochemical properties of *Botryllus schlosseri* haemocytes: indications for morpho-functional characterisation. Eur. J. Histochem 49, 255–264. [PubMed: 16216811]

Ballarin L, Menin A, Tallandini L, Matozzo V, Burighel P, Basso G, Fortunato E, and Cima F (2008). Haemocytes and blastogenetic cycle in the colonial ascidian *Botryllus schlosseri*: a matter of life and death. Cell Tissue Res 331, 555–564. [PubMed: 17972103]

Ben-Ari Fuchs S, Lieder I, Stelzer G, Mazor Y, Buzhor E, Kaplan S, Bogoch Y, Plaschkes I, Shitrit A, Rappaport N, et al. (2016). Geneanalytics: an integrative gene set analysis tool for next generation sequencing, rnaseq and microarray data. OMICS 20, 139–151. [PubMed: 26983021]

Bosch TC (2009). Hydra and the evolution of stem cells. BioEssays 31, 478–486. [PubMed: 19274660]

Boyd HC, Brown SK, Harp JA, and Weissman IL (1986). Growth and Sexual Maturation of Laboratory-Cultured Monterey California Usa Botryllus-Schlosseri. Biological Bulletin 170, 91–109.

Brown FD, Tiozzo S, Roux MM, Ishizuka K, Swalla BJ, and De Tomaso AW (2009). Early lineage specification of long-lived germline precursors in the colonial ascidian *Botryllus schlosseri*. Development 136, 3485–3494. [PubMed: 19783737]

Brunetti R, and Burighel P (1969). Sviluppo dell'apparato vascolare coloniale in Botryllus schlosseri (Pallas). Pubbl. Stn. Zool. Napoli 37, 137–148.

Burighel P, and Brunetti R (1971). The circulatory system in the blastozooid of the colonial ascidian *Botryllus schlosseri* (Pallas). Italian Journal of Zoology 38, 273–289.

Burighel P, and Cloney RA (1997). Urochordata: Ascidiacea. In Microscopic Anatomy of Invertebrates, Harrison FW and Ruppert EE, eds. (Wiley-Liss), pp. 221–347.

Burighel P, Milanesi C, and Sabbadin A (1983). Blood cell ultrastructure of the ascidian *Botryllus schlosseri* L. II. Pigment cells. Acta Zool 64, 15–23.

Caicci F, Zaniolo G, Burighel P, Degasperi V, Gasparini F, and Manni L (2010). Differentiation of papillae and rostral sensory neurons in the larva of the ascidian *Botryllus schlosseri* (Tunicata). J. Comp. Neurol 518, 547–566. [PubMed: 20020541]

Cañestro C, Bassham S, and Postlethwait JH (2008). Evolution of the thyroid: anterior-posterior regionalization of the *Oikopleura* endostyle revealed by *Otx*, *Pax2/5/8*, and *Hox1* expression. Dev. Dyn 237, 1490–1499. [PubMed: 18386819]

Cao C, Lemaire LA, Wang W, Yoon PH, Choi YA, Parsons LR, Matese JC, Wang W, Levine M, and Chen K (2019). Comprehensive single-cell transcriptome lineages of a proto-vertebrate. Nature 571, 349–354. [PubMed: 31292549]

Castrillon DH, Quade BJ, Wang TY, Quigley C, and Crum CP (2000). The human *VASA* gene is specifically expressed in the germ cell lineage. Proc. Natl. Acad. Sci. USA 97, 9585–9590. [PubMed: 10920202]

Chan M, Smith ZD, Grosswendt S, Kretzmer H, Norman T, Adamson B, Jost M, Quinn JJ, Yang D, Meissner A, et al. (2018). Molecular recording of mammalian embryogenesis. BioRxiv

Chiquoine AD (1954). The identification, origin, and migration of the primordial germ cells in the mouse embryo. Anat. Rec 118, 135–146. [PubMed: 13138919]

Conklin E (1905). The Organization and Cell-Lineage of the Ascidian Egg (Academy of Natural Sciences of Philadelphia).

Cox DN, Chao A, and Lin H (2000). piwi encodes a nucleoplasmic factor whose activity modulates the number and division rate of germline stem cells. Development 127, 503–514. [PubMed: 10631171]

Davidson EH, Rast JP, Oliveri P, Ransick A, Calestani C, Yuh CH, Minokawa T, Amore G, Hinman V, Arenas-Mena C, et al. (2002). A genomic regulatory network for development. Science 295, 1669–1678. [PubMed: 11872831]

Dixon KE (1994). Evolutionary aspects of primordial germ cell formation. Ciba Found. Symp 182, 92–110, discussion 110–120. [PubMed: 7835159]

Dobin A, Davis CA, Schlesinger F, Drenkow J, Zaleski C, Jha S, Batut P, Chaisson M, and Gingeras TR (2013). STAR: ultrafast universal RNA-seq aligner. Bioinformatics 29, 15–21. [PubMed: 23104886]

Duboule D (1994). Temporal colinearity and the phylotypic progression: a basis for the stability of a vertebrate Bauplan and the evolution of morphologies through heterochrony. Dev. Suppl 1994, 135–142.

Farley EK, Olson KM, Zhang W, Brandt AJ, Rokhsar DS, and Levine MS (2015). Suboptimization of developmental enhancers. Science 350, 325–328. [PubMed: 26472909]

Farrell JA, Wang Y, Riesenfeld SJ, Shekhar K, Regev A, and Schier AF (2018). Single-cell reconstruction of developmental trajectories during zebrafish embryogenesis. Science 360, eaar3131.

Gasparini F, Shimeld SM, Ruffoni E, Burighel P, and Manni L (2011). Expression of a Musashi-like gene in sexual and asexual development of the colonial chordate *Botryllus schlosseri* and phylogenetic analysis of the protein group. J. Exp. Zoolog. B Mol. Dev. Evol 316, 562–573.

Gasparini F, Caicci F, Rigon F, Zaniolo G, and Manni L (2014). Testing an unusual in vivo vessel network model: a method to study angiogenesis in the colonial tunicate *Botryllus schlosseri*. Sci. Rep 4, 6460. [PubMed: 25248762]

Ginsburg M, Snow MH, and McLaren A (1990). Primordial germ cells in the mouse embryo during gastrulation. Development 110, 521–528. [PubMed: 2133553]

Grave C, and Woodbridge H (1924). *Botryllus schlosseri* (Pallas): the behavior and morphology of the free? swimming larva. J. Morphol. Physiol 39, 207–247.

Grosberg RK, and Quinn JF (1986). The genetic control and consequences of kin recognition by the larvae of a colonial marine invertebrate. Nature 322, 456–459.

Harris CR, Millman KJ, van der Walt SJ, Gommers R, Virtanen P, Cournapeau D, Wieser E, Taylor J, Berg S, Smith NJ, et al. (2020). Array programming with NumPy. Nature 585, 357–362. [PubMed: 32939066]

Hotta K, Mitsuhara K, Takahashi H, Inaba K, Oka K, Gojobori T, and Ikeo K (2007). A web-based interactive developmental table for the ascidian *Ciona intestinalis*, including 3D real-image embryo reconstructions: I. From fertilized egg to hatching larva. Dev. Dyn 236, 1790–1805. [PubMed: 17557317]

Hu H, Uesaka M, Guo S, Shimai K, Lu T-M, Li F, Fujimoto S, Ishikawa M, Liu S, Sasagawa Y, et al.; EXPANDE Consortium (2017). Constrained vertebrate evolution by pleiotropic genes. Nat. Ecol. Evol 1, 1722–1730. [PubMed: 28963548]

Hunter JD (2007). Matplotlib: A 2D Graphics Environment. Computing in Science & Engineering 9, 90–95.

Irie N, and Kuratani S (2011). Comparative transcriptome analysis reveals vertebrate phylotypic period during organogenesis. Nat. Commun 2, 248. [PubMed: 21427719]

Jagannathan-Bogdan M, and Zon LI (2013). Hematopoiesis. Development 140, 2463–2467. [PubMed: 23715539]

Karaiskou A, Swalla BJ, Sasakura Y, and Chambon J-P (2015). Metamorphosis in solitary ascidians. Genesis 53, 34–47. [PubMed: 25250532]

Kawaminani S, and Nishida H (1997). Induction of trunk lateral cells, the blood cell precursors, during ascidian embryogenesis. Dev. Biol 181, 14–20. [PubMed: 9015261]

Kawamura K, Tiozzo S, Manni L, Sunanaga T, Burighel P, and De Tomaso AW (2011). Germline cell formation and gonad regeneration in solitary and colonial ascidians. Dev. Dyn 240, 299–308. [PubMed: 21246647]

Köster J, and Rahmann S (2012). Snakemake—a scalable bioinformatics workflow engine. Bioinformatics 28, 2520–2522. [PubMed: 22908215]

Krumlauf R (1994). Hox genes in vertebrate development. Cell 78, 191–201. [PubMed: 7913880]

Laird DJ, De Tomaso AW, and Weissman IL (2005). Stem cells are units of natural selection in a colonial ascidian. Cell 123, 1351–1360. [PubMed: 16377573]

Lambert SA, Jolma A, Campitelli LF, Das PK, Yin Y, Albu M, Chen X, Taipale J, Hughes TR, and Weirauch MT (2018). The human transcription factors. Cell 172, 650–665. [PubMed: 29425488]

Langmead B, and Salzberg SL (2012). Fast gapped-read alignment with Bowtie 2. Nat. Methods 9, 357–359. [PubMed: 22388286]

Lauzon RJ, Patton CW, and Weissman IL (1993). A morphological and immunohistochemical study of programmed cell death in *Botryllus schlosseri* (Tunicata, Ascidiacea). Cell Tissue Res 272, 115–127. [PubMed: 8386984]

Lee MT, Bonneau AR, Takacs CM, Bazzini AA, DiVito KR, Fleming ES, and Giraldez AJ (2013). Nanog, Pou5f1 and SoxB1 activate zygotic gene expression during the maternal-to-zygotic transition. Nature 503, 360–364. [PubMed: 24056933]

Leggio B, Laussu J, Carlier A, Godin C, Lemaire P, and Faure E (2019). MorphoNet: an interactive online morphological browser to explore complex multi-scale data. Nat. Commun 10, 2812. [PubMed: 31249294]

Manni L, and Pennati R (2015). Tunicata. Structure and Evolution of Invertebrate Nervous Systems (Oxford University Press), pp. 699–718.

Manni L, Lane NJ, Sorrentino M, Zaniolo G, and Burighel P (1999). Mechanism of neurogenesis during the embryonic development of a tunicate. J. Comp. Neurol 412, 527–541. [PubMed: 10441238]

Manni L, Gasparini F, Hotta K, Ishizuka KJ, Ricci L, Tiozzo S, Voskoboynik A, and Dauga D (2014). Ontology for the asexual development and anatomy of the colonial chordate *Botryllus schlosseri*. PLoS ONE 9, e96434. [PubMed: 24789338]

Li H, and Durbin R (2009). Fast and accurate short read alignment with Burrows-Wheeler transform. Bioinformatics 25, 1754–1760. [PubMed: 19451168]

Li H, Handsaker B, Wysoker A, Fennell T, Ruan J, Homer N, Marth G, Abecasis G, and Durbin R; 1000 Genome Project Data Processing Subgroup (2009). The Sequence Alignment/Map format and SAMtools. Bioinformatics 25, 2078–2079. [PubMed: 19505943]

Manni L, Anselmi C, Cima F, Gasparini F, Voskoboynik A, Martini M, Peronato A, Burighel P, Zaniolo G, and Ballarin L (2019). Sixty years of experimental studies on the blastogenesis of the colonial tunicate *Botryllus schlosseri*. Dev. Biol 448, 293–308. [PubMed: 30217596]

Marani E, van Oers JW, Tetteroo PA, Poelmann RE, van der Veeken J, and Deenen MG (1986). Stage specific embryonic carbohydrate surface antigens of primordial germ cells in mouse embryos: FAL (S.S.E.A.−1) and globoside (S.S.E.A.−3). Acta Morphol. Neerl. Scand 24, 103–110. [PubMed: 2882649]

Marlétaz F, Firbas PN, Maeso I, Tena JJ, Bogdanovic O, Perry M, Wyatt CDR, de la Calle-Mustienes E, Bertrand S, Burguera D, et al. (2018). Amphioxus functional genomics and the origins of vertebrate gene regulation. Nature 564, 64–70. [PubMed: 30464347]

Milanesi C, and Burighel P (1978). Blood cell ultrastructure of the ascidian *Botryllus schlosseri*. Acta Zool 59, 135–147.

Nishida H, and Stach T (2014). Cell lineages and fate maps in tunicates: conservation and modification. Zool. Sci 31, 645–652.

Nowotschin S, Setty M, Kuo Y-Y, Liu V, Garg V, Sharma R, Simon CS, Saiz N, Gardner R, Boutet SC, et al. (2019). The emergent landscape of the mouse gut endoderm at single-cell resolution. Nature 569, 361–367. [PubMed: 30959515]

Ogasawara M, Lauro R, and Satoh N (1999). Ascidian homologs of mammalian thyroid transcription factor-1 gene are expressed in the endostyle. Zoolog. Sci 16, 559–565.

Ohno S (1970). Evolution by Gene Duplication (Springer).

Prummel KD, Hess C, Nieuwenhuize S, Parker HJ, Rogers KW, Kozmikova I, Racioppi C, Brombacher EC, Czarkwiani A, Knapp D, et al. (2019). A conserved regulatory program initiates lateral plate mesoderm emergence across chordates. Nat. Commun 10, 3857. [PubMed: 31451684]

Raz E (2000). The function and regulation of vasa-like genes in germ-cell development. Genome Biol 1, REVIEWS1017.

Rinkevich Y, Voskoboynik A, Rosner A, Rabinowitz C, Paz G, Oren M, Douek J, Alfassi G, Moiseeva E, Ishizuka KJ, et al. (2013). Repeated, long-term cycling of putative stem cells between niches in a basal chordate. Dev. Cell 24, 76–88. [PubMed: 23260626]

Robinson MD, McCarthy DJ, and Smyth GK (2010). edgeR: a Bioconductor package for differential expression analysis of digital gene expression data. Bioinformatics 26, 139–140. [PubMed: 19910308]

Rosental B, Kowarsky M, Seita J, Corey DM, Ishizuka KJ, Palmeri KJ, Chen S-Y, Sinha R, Okamoto J, Mantalas G, et al. (2018). Complex mammalian-like haematopoietic system found in a colonial chordate. Nature 564, 425–429. [PubMed: 30518860]

Rosner A, Moiseeva E, Rinkevich Y, Lapidot Z, and Rinkevich B (2009). Vasa and the germ line lineage in a colonial urochordate. Dev. Biol 331, 113–128. [PubMed: 19406116]

Sabbadin A (1955). Studies on blood cells in *Botryllus schlosseri* (Pallas). Arch. Ital. Anat. Embriol 60, 33–67. [PubMed: 14377796]

Sabbadin A, and Zaniolo G (1979). Sexual differentiation and germ cell transfer in the colonial ascidian Botryllus schlosseri. J. Exp. Zool 207, 289–304.

Saitou M, Payer B, O'Carroll D, Ohinata Y, and Surani MA (2005). Blimp1 and the emergence of the germ line during development in the mouse. Cell Cycle 4, 1736–1740. [PubMed: 16294024]

Satou Y, and Satoh N (1999). Developmental gene activities in ascidian embryos. Curr. Opin. Genet. Dev 9, 542–547. [PubMed: 10508695]

Schaum N, Karkanias J, Neff NF, May AP, Quake SR, Wyss-Coray T, Darmanis S, Batson J, Botvinnik O, Chen MB, et al.; Tabula Muris Consortium; Overall coordination; Logistical coordination; Organ collection and processing; Library preparation and sequencing; Computational data analysis; Cell type annotation; Writing group; Supplemental text writing group; Principal investigators (2018). Single-cell transcriptomics of 20 mouse organs creates a *Tabula Muris*. Nature 562, 367–372. [PubMed: 30283141]

Shirae-Kurabayashi M, Nishikata T, Takamura K, Tanaka KJ, Nakamoto C, and Nakamura A (2006). Dynamic redistribution of vasa homolog and exclusion of somatic cell determinants during germ cell specification in Ciona intestinalis. Development 133, 2683–2693. [PubMed: 16794033]

Simakov O, Marlétaz F, Yue J-X, O'Connell B, Jenkins J, Brandt A, Calef R, Tung C-H, Huang T-K, Schmutz J, et al. (2020). Deeply conserved synteny resolves early events in vertebrate evolution. Nat. Ecol. Evol 4, 820–830. [PubMed: 32313176]

Soriano P, and Jaenisch R (1986). Retroviruses as probes for mammalian development: allocation of cells to the somatic and germ cell lineages. Cell 46, 19–29. [PubMed: 3013418]

Sorrentino M, Manni L, Lane NJ, and Burighel P (2000). Evolution of cerebral vesicles and their sensory organs in an ascidian larva. Acta Zool 81, 243–258.

Spangrude GJ, Heimfeld S, and Weissman IL (1988). Purification and characterization of mouse hematopoietic stem cells. Science 241, 58–62. [PubMed: 2898810]

Spemann H, and Mangold H (2001). Induction of embryonic primordia by implantation of organizers from a different species. 1923. Int. J. Dev. Biol 45, 13–38. [PubMed: 11291841]

Stach T, and Anselmi C (2015). High-precision morphology: bifocal 4D-microscopy enables the comparison of detailed cell lineages of two chordate species separated for more than 525 million years. BMC Biol 13, 113. [PubMed: 26700477]

Stoner DS, and Weissman IL (1996). Somatic and germ cell parasitism in a colonial ascidian: possible role for a highly polymorphic allorecognition system. Proc. Natl. Acad. Sci. USA 93, 15254–15259. [PubMed: 8986797]

Stoner DS, Rinkevich B, and Weissman IL (1999). Heritable germ and somatic cell lineage competitions in chimeric colonial protochordates. Proc. Natl. Acad. Sci. USA 96, 9148–9153. [PubMed: 10430910]

Sulston JE, Schierenberg E, White JG, and Thomson JN (1983). The embryonic cell lineage of the nematode *Caenorhabditis elegans*. Dev. Biol 100, 64–119. [PubMed: 6684600]

Tiozzo S, Christiaen L, Deyts C, Manni L, Joly J-S, and Burighel P (2005). Embryonic versus blastogenetic development in the compound ascidian *Botryllus schlosseri*: insights from *Pitx* expression patterns. Dev. Dyn 232, 468–478. [PubMed: 15614778]

Ueno H, Turnbull BB, and Weissman IL (2009). Two-step oligoclonal development of male germ cells. Proc. Natl. Acad. Sci. USA 106, 175–180. [PubMed: 19098099]

Voskoboynik A, Simon-Blecher N, Soen Y, Rinkevich B, De Tomaso AW, Ishizuka KJ, and Weissman IL (2007). Striving for normality: whole body regeneration through a series of abnormal generations. FASEB J 21, 1335–1344. [PubMed: 17289924]

Voskoboynik A, Soen Y, Rinkevich Y, Rosner A, Ueno H, Reshef R, Ishizuka KJ, Palmeri KJ, Moiseeva E, Rinkevich B, and Weissman IL (2008). Identification of the endostyle as a stem cell niche in a colonial chordate. Cell Stem Cell 3, 456–464. [PubMed: 18940736]

Voskoboynik A, Neff NF, Sahoo D, Newman AM, Pushkarev D, Koh W, Passarelli B, Fan HC, Mantalas GL, Palmeri KJ, et al. (2013a). The genome sequence of the colonial chordate, *Botryllus schlosseri*. eLife 2, e00569. [PubMed: 23840927]

Voskoboynik A, Newman AM, Corey DM, Sahoo D, Pushkarev D, Neff NF, Passarelli B, Koh W, Ishizuka KJ, Palmeri KJ, et al. (2013b). Identification of a colonial chordate histocompatibility gene. Science 341, 384–387. [PubMed: 23888037]

Wagner DE, Weinreb C, Collins ZM, Briggs JA, Megason SG, and Klein AM (2018). Single-cell mapping of gene expression landscapes and lineage in the zebrafish embryo. Science 360, 981–987. [PubMed: 29700229]

Weismann A (1892). Das Keimplasma: Eine Theorie der Vererbung (Gustav Fischer).

Weissman IL (2015). Stem cells are units of natural selection for tissue formation, for germline development, and in cancer development. Proc. Natl. Acad. Sci. USA 112, 8922–8928. [PubMed: 26195745]

Zaniolo G, Lane NJ, Burighel P, and Manni L (2002). Development of the motor nervous system in ascidians. J. Comp. Neurol 443, 124–135. [PubMed: 11793351]

Highlights

- Embryogenesis and blastogenesis have different morphological and molecular programs
- Distinct molecular programs can lead to the same outcome
- Tissue-specific transcriptional timings are shared in both developmental pathways
- The expression and timing of many transcription factors are conserved in development

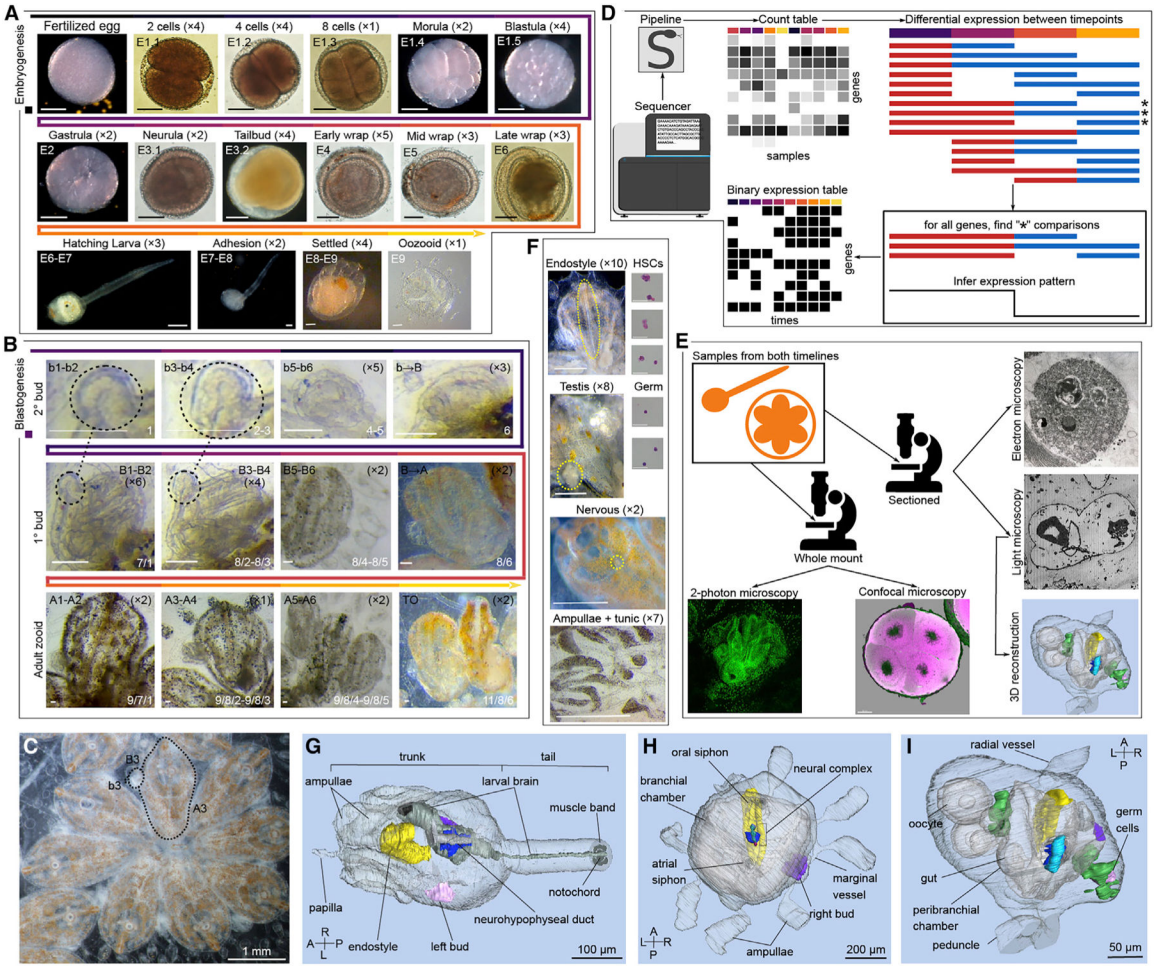

Figure 1. Sampling and methods for compiling the *B. schlosseri* atlas

(A) The embryonic pathway from a fertilized egg until after metamorphosis. Numbers in parentheses indicate the number of samples used in the transcriptomic analysis. Labels on the images indicate the developmental stage. Scale bars: 100 μm for the top two rows, 60 μm for the lower row.

(B) The blastogenic pathway for three generations (secondary buds [b], primary buds [B], and adult zooids [A]). Dotted circles and lines indicate that samples were collected together. Labels on images indicate the developmental stage based on the days of development (see STAR methods) and the staging according Sabbadin (1995) (white labels). Scale bars represent 100 μm.

(C) *B. schlosseri* colony. The dotted lines highlight an adult (A3), with a primary bud (B3) and secondary bud (b3).

(D) Description of pipeline for determining developmentally dynamic genes. Sequenced reads are processed to produce a gene count table. Samples from different sets of time (red versus blue) are compared, differentially expressed genes (*) are gathered, and the optimal binary expression pattern is inferred.

(E) Methods used to build the morphological atlas.

(F) Various tissues and cell populations used in the transcriptome analysis. Scale bars (tissues), 100 μm; scale bars (cells), 40 μm.
(G–I) 3D reconstruction of (G) a larva in early metamorphosis (E8); (H) an oozooid (E9), with its secondary bud (b4); and (I) a bud (B1) with its secondary bud (b1), in which the outer epithelium is the epidermis. Cerebral ganglion, blue; dorsal organ, burgundy; dorsal tube, light blue; endostyle, yellow; germ cells, light pink; larval nervous system, dark gray; left bud, stage b1, light violet; neural gland, green; neural gland aperture, purple; neurohypophyseal duct, light gray; photolith, black; right bud, advanced stage b1, dark violet; testis, green. Other structures are transparent. Dorsal view.
See also Figures S1 and S2, Tables S1, S2, and S3, and Methods S1.

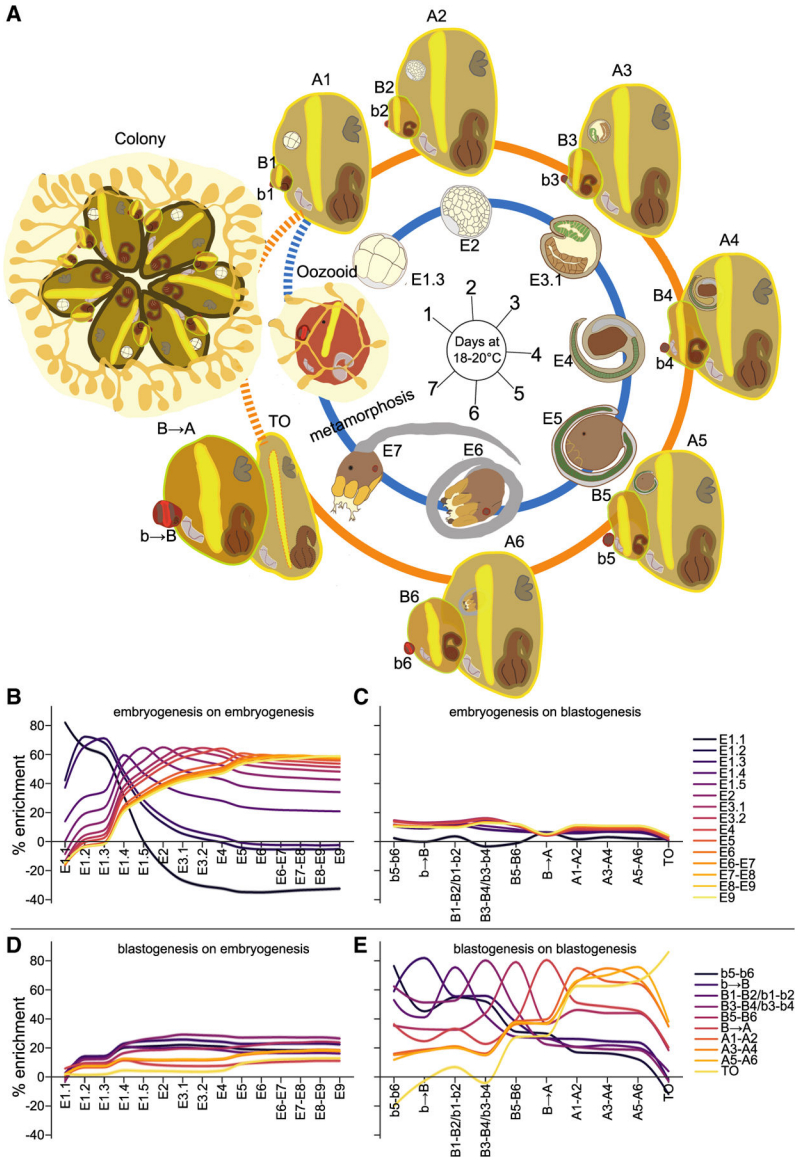

Figure 2. *B. schlosseri* life cycle: morpho-logical and molecular changes across and between developmental pathways

(A) Sexual and asexual stages of development are synchronized. Embryogenesis begins with a zygote that develops into a swimming larva (E7; day 7). The larva settles on a substrate (E8-E9), and metamorphoses into an oozoid (E9). During the embryonic phase a bud is also developed and remains after metamorphosis in the oozooid as the precursors for the next-generation zooid. The weekly asexual budding cycle begins with secondary buds (b1–b6) that grow into primary buds (b→B), which in turn complete organogenesis (B1–B6) and replace their parent zooid (B→A). Zooids open their siphons and live for 6 days (A1–A6); on day 7 all of the zooids in the colony undergo a synchronized programmed cell death and removal and are cleared through phagocytosis (takeover [TO]). Larvae hatch on day 6 before the TO stage. When a zooid grows more than one bud, a colony of genetically identical zooids is produced. Embryogenesis, blue line; blastogenesis, orange line. Key organs depicted include notochord (green), pharynx (light brown), ampullae (orange), papillae

(light yellow), endostyle (yellow), stomach (brown), testes (mauve), heart (pink), and circulatory system (orange). A solid versus dashed line indicates a continuous versus discrete time point.

(B–E) Enrichment plots (see Methods S2) of expressed developmentally dynamic genes at each stage of embryogenesis (B and C) and blastogenesis (D and E) are shown compared to the gene sets expressed at all other stages in embryogenesis (B and D) and blastogenesis (C and E). (B) and (E) show the patterns of similarity within a pathway, with enrichment decreasing as time from a gene set increases. (C) and (D) show the comparative low levels of similarity between embryogenesis and blastogenesis.

See also Tables S3, S4, and S5 and Methods S2.

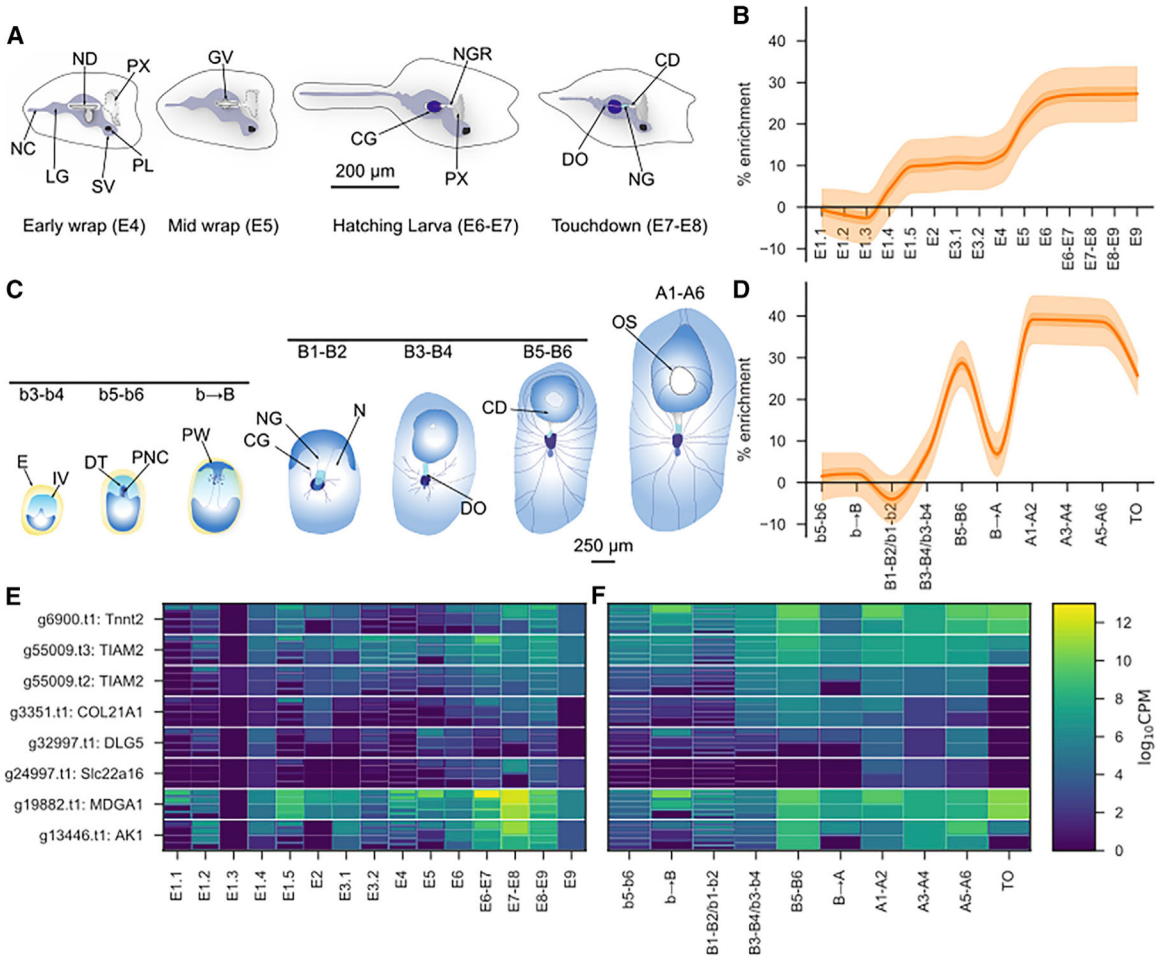

Figure 3. Origin and development of the nervous system

(A) Schematic illustration of nervous system development during embryogenesis (early wrap [E4] to settled larva [E7–E8]). NC, nerve cord; LG, larval ganglion; SV, sensory vesicle; PL, photolith; PX, pharynx; ND, neurohypophyseal duct; GV, ganglionic vesicle; NGR, neural gland rudiment; CG, cerebral ganglion; CD, ciliated duct; DO, dorsal organ; NG, neural gland.

(B) Gene enrichment plot of CNS-associated genes during embryogenesis. Light and dark shaded regions indicate the 50% and 99% confidence intervals under a hypergeometric model.

(C) Schematic illustration of nervous system development during blastogenesis (b3–b4 to A1–A6). LE, epidermis; IV, inner vesicle; DT, dorsal tube; PNC, pioneer nerve cell; PW, pharyngeal wall; CG, cerebral ganglion; NT, neural gland; N, nerve; DO, dorsal organ; CD, ciliated duct; OS, oral siphon.

(D) Gene enrichment plot of CNS-associated genes during blastogenesis.

(E and F) Klee plots (heatmaps) of putative transcription factors found to be dynamic between E4 and E7 that are expressed in the nervous system and associated with nervous system development. For Klee plots (heatmaps), around and between each grouping the mean value of the group is shown in the outline.

(E) Embryogenesis.

(F) Blastogenesis.

See also Figure S3 and Tables S1, S2, S3, S4, S5, and S6.

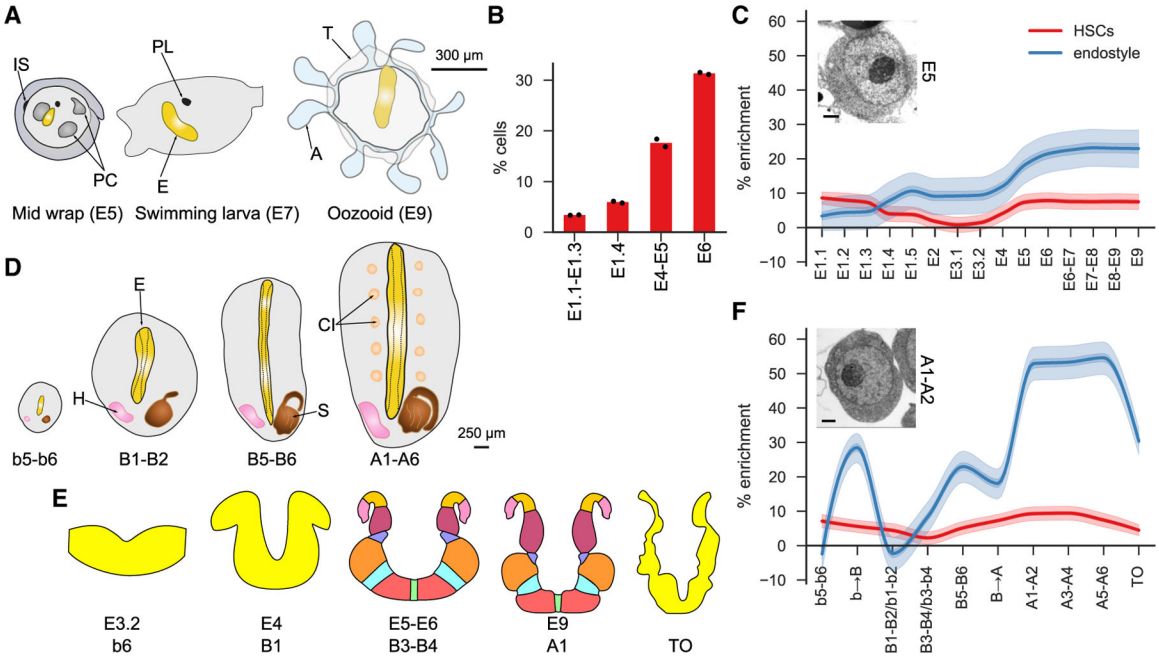

Figure 4. Origin and development of hematopoiesis and its niche (endostyle)

(A) Illustration of the endostyle development during embryogenesis (mid wrap [E5] to oozooid [E9]). IS, interpapillary space; PC, peribranchial chamber; PL, photolith; E, endostyle; T, tunic; A, ampulla.

(B) Proportion of cells in embryos that are identified as enriched for HSCs using a fluorescence-activated cell sorting (FACS)-based assay.

(C) Gene enrichment plot of HSCs and endostyle-associated genes during embryogenesis. Inset is a transmission electron microscopy (TEM) image of a hemoblast.

(D) Schematic illustration of endostyle development during blastogenesis (b5–b6 to A1–A6). H, heart; E, endostyle; S, stomach; CI, cell island.

(E) Illustration of a transverse section of the endostyle during development in both embryogenesis and blastogenesis. See details in Figure S4.

(F) Gene enrichment plot of cells enriched for HSC and endostyle-associated genes during blastogenesis. Inset is an adult zooid's hemoblast. Scale bar, 1 µm.

See also Figure S4 and Tables S1, S2, S3, S4, S5, and S6.

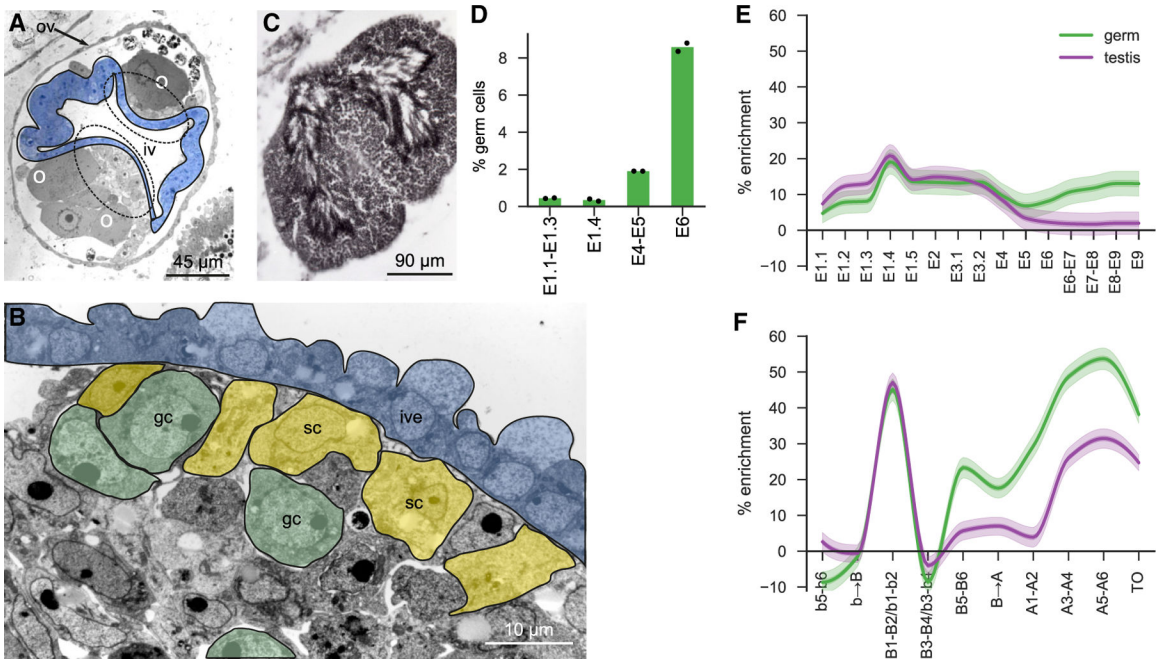

Figure 5. Origin and development of germ cells and the testis

(A) Transverse section of secondary bud (b5) with bilateral gonad rudiment (dotted lines) pressing inner vesicle (iv, blue) and gonadal blastema. Some previtellogenic oocytes (O) are close to the epidermis, the outer vesicle (ov). Toluidine blue.

(B) Candidate male primordial germ cells (gc, green) are grouped together with presumptive somatic cells (sc, yellow). They are close to the inner vesicle epithelium (ive, blue). TEM.

(C) Section of an adult zooid testis lobule. Immature germ cells are at testis periphery; mature sperms are central. Toluidine blue.

(D) Proportion of cells in embryos that are identified as germ cells using a FACS-based assay.

(E and F) Gene enrichment plot of germ- and testis-associated genes during embryogenesis (E) and blastogenesis (F).

See also Figure S5 and Tables S1, S2, S3, S4, S5, and S6.

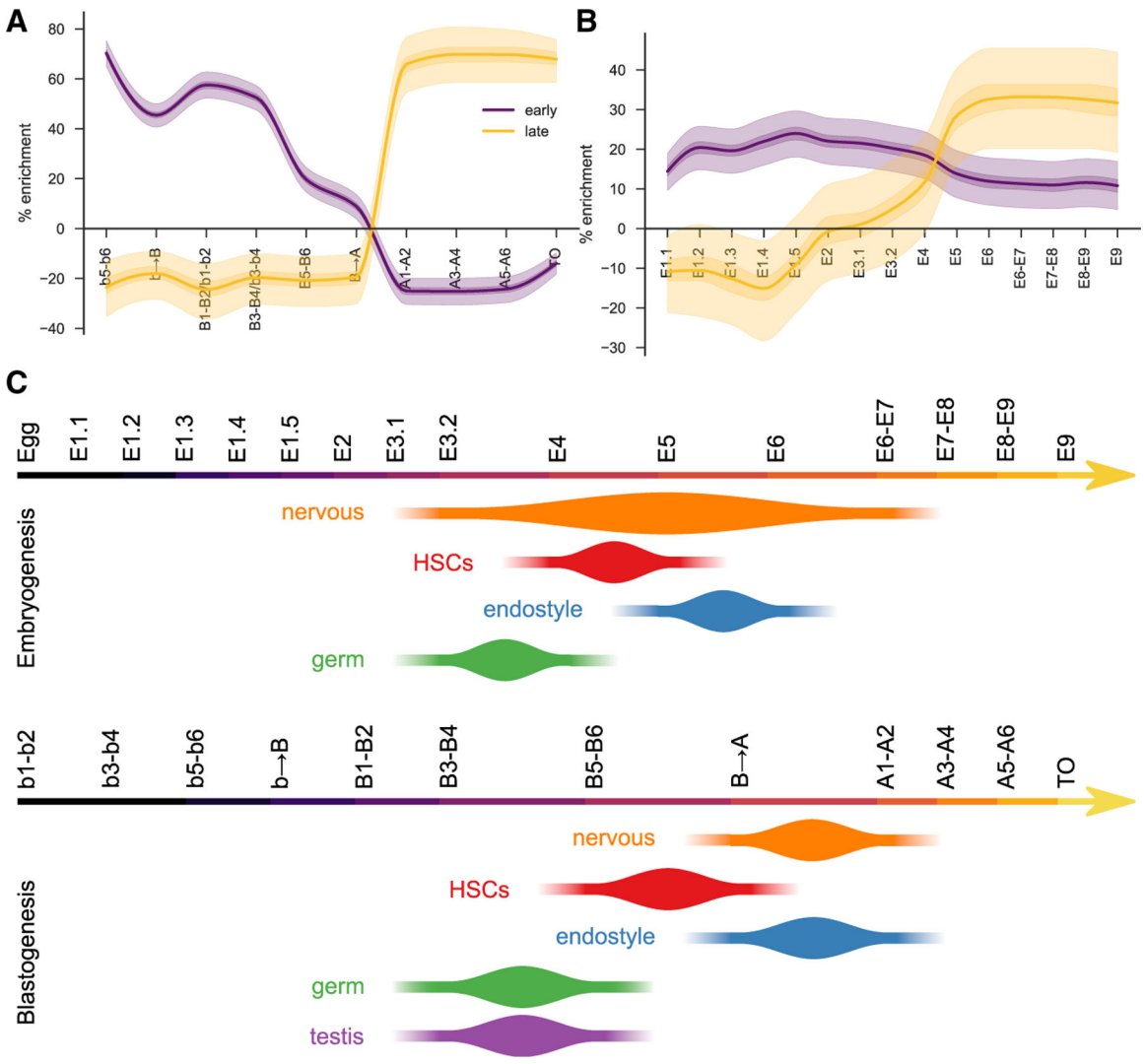

Figure 6. Timeline of organogenesis inferred from transcriptional signatures

(A) Gene enrichment plot of early (expressed only up to B→A) and late (expressed only after B→A) HSC-associated genes during blastogenesis. Baseline (0%) is set under the null model of a random subset of genes. Light and dark shaded regions indicate the 50% and 99% confidence intervals under a hypergeometric model.

(B) Gene enrichment plot of the same sets of genes as shown in (A), but during embryogenesis.

(C) Estimated regions in organ development of the transition between early/late shared gene expression.

See also Figure S6 and Tables S1, S2, S3, S4, S5, and S6.

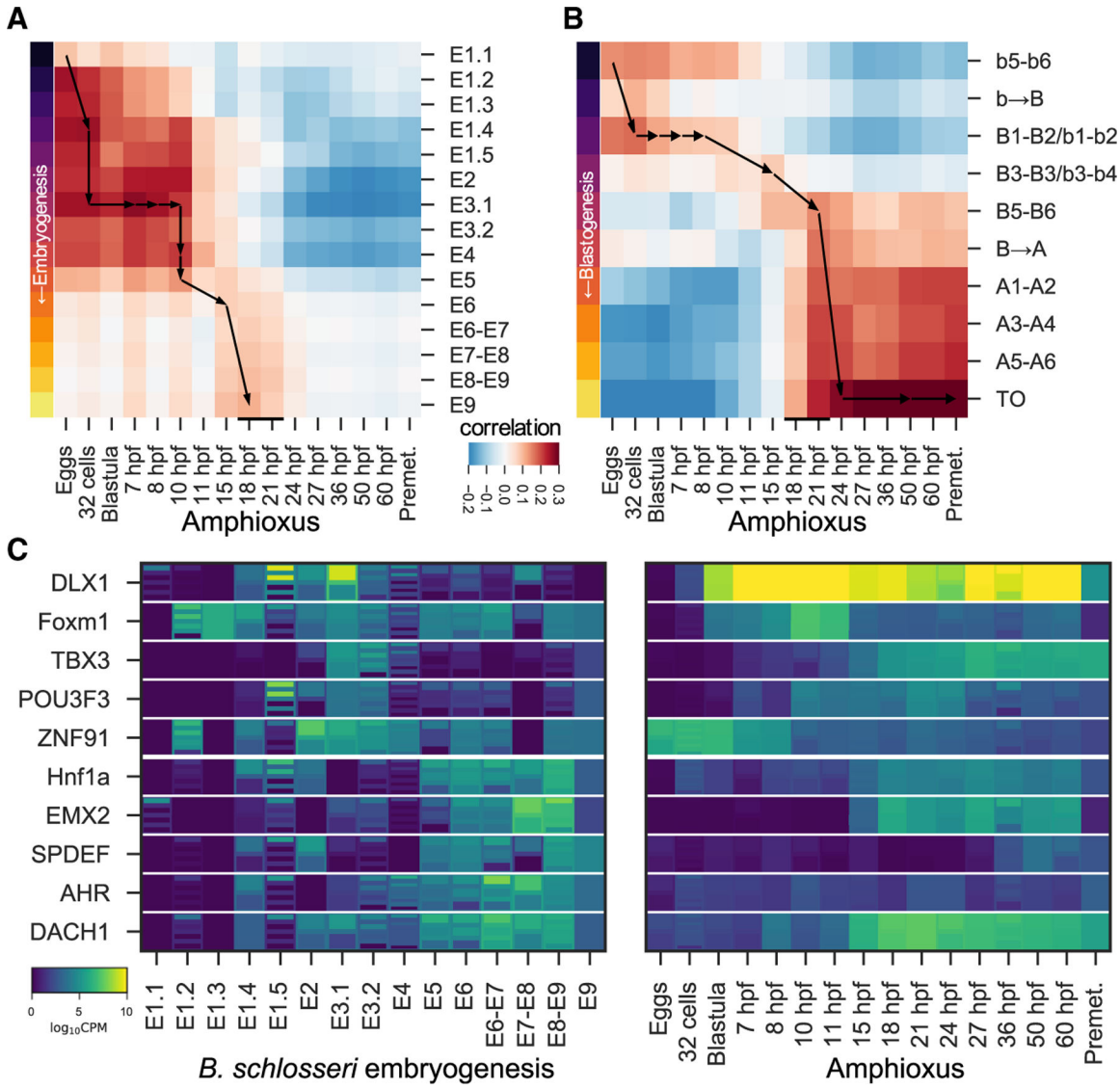

Figure 7. Comparison between *B. schlosseri* developmental pathways and amphioxus embryogenesis

(A) Correlation between shared transcription factors at various time points between embryogenesis in *B. schlosseri* (rows) and in amphioxus (columns). Arrows indicate the estimated path of equivalent times in the two pathways. The phylotypic period in amphioxus is 18–21 hpf and indicated by a thin black bar.

(B) Similar to (A), but for blastogenesis in *B. schlosseri*.

(C) Klee plot of the top (by fold change) transcription factors shared between species (*B. schlosseri* and amphioxus) that are co-expressed either early (upper 5) or late (lower 5) (see Figure 2E) in embryogenesis and blastogenesis in *B. schlosseri*.

See also Figure S7 and Table S7.

KEY RESOURCES TABLE

REAGENT or RESOURCE	SOURCE	IDENTIFIER
Antibodies		
Monoclonal anti-alpha-tubulin	Sigma Aldrich	Cat#T5168
Anti-mouse fluorescein conjugated	Calbiochem	Cat#401234
Alexa Fluor 546 Phalloidin	Invitrogen	A22283
DAPI	Sigma	Cat#D9542
Propidium Iodide	Invitrogen	#R37169
Alkaline Phosphatase Live Stain	Life Technologies	A14353
Chemicals, peptides, and recombinant proteins		
Quick RNA MIcro Prep Kit	Zymo	# R1050
RNA Clean and Concentrator	Zymo	#R1015
Nugen Ovation RNA Sequencing System V2	Nugen	#7102
QIAGEN QIAquick PCR purification kit	QIAGEN	#28104
Select-A-Size DNA Clean and Concentrator	Zymo	#D4080
NEBNext Ultra II DNA Library Prep Kit	NEB	#27645
NEBNext Multiplex Oligos for Illumina	NEB	#E6609S
BullDogBio CleanNGS RNA and DNA Spri Beads	BullDogBio	#CNGS005
Deposited data		
The sequencing data generated during this study are available on the NCBI Sequence Read Archive under accession: PRJNA579844.	NCBI	PRJNA579844
Three dimensional reconstructions of Botryllus larvae and buds	morphonet browser	https://morphonet.org Login: Botryllus3D Password: oozooid
Experimental models: organisms/strains		
Botryllus schlosseri family Botryllidae, order Stolidobranchiata	Venice Lagoon (IT)	N/A
Botryllus schlosseri family Botryllidae, order Stolidobranchiata	Monterey Bay (CA)	N/A
Botryllus schlosseri family Botryllidae, order Stolidobranchiata	Weissman lab mariculture HMS	N/A
Software and algorithms		
Amira 5.3.3 3D Visualization & Analysis Software	Thermo Fisher	N/A
BWA	Li and Durbin, (2009)	https://github.com/lh3/bwa
Samtools	Li et al., (2009)	http://www.htslib.org/
Numpy and scipy	Harris et al., (2020)	https://numpy.org/
Matplotlib	Hunter, (2007)	https://matplotlib.org/
Snakemake	Köster and Rahmann (2012)	https://snakemake.github.io/
Bowtie2	Langmead and Salzberg (2012)	http://bowtie-bio.sourceforge.net/bowtie2/index.shtml

REAGENT or RESOURCE	SOURCE	IDENTIFIER
STAR	Dobin et al. (2013)	https://github.com/alexdobin/STAR
edgeR	Robinson et al. (2010)	http://bioconductor.org/packages/release/bioc/html/edgeR.html
Python code - Identification of developmentally dynamic genes and formation of binary tables	This paper	Methods S1
Python code- Gene enrichment plots	This paper	Methods S2
Other		
GeneAnalytics	Ben-Ari Fuchs et al. (2016)	https://geneanalytics.genecards.org/